

Fifth International Conference

# MMM 2010

## Multiscale Materials Modeling

October 04 - 08, 2010, Freiburg, Germany

### CONFERENCE PROCEEDINGS

Editors:  
Peter Gumbsch  
Erik van der Giessen

FRAUNHOFER VERLAG

Organized by Fraunhofer Institute  
for Mechanics of Materials IWM.  
Hosted by University of Freiburg.



Supported by



# *Multifunctional Materials*



# Low-voltage, high-mobility transparent oxide transistors fabricated by spray coating

George Adamopoulos

Department of Physics, Blackett Laboratory, Imperial College London, SW7 2BW, London, UK

The downscaling of the complementary metal oxide semiconductor (CMOS) transistors has led to very thin dielectric layers that resulted in unacceptably high leakage currents. The need of replacing silicon dioxide ( $\text{SiO}_2$ ) - the standard dielectric used- with physically thicker layers of higher dielectric constant led to the investigation of new dielectrics such as zirconium oxide ( $\text{ZrO}_2$ ) and yttrium oxide ( $\text{Y}_2\text{O}_3$ ) with inferior properties than  $\text{SiO}_2$ . On the other hand the high optical transparency and excellent charge transport characteristics combined with their excellent chemical stability and mechanical tolerance make oxide semiconductors attractive for applications in large area optoelectronics and particularly thin-film transistors (TFTs). However, the vast majority of high performance oxide-based transistors reported so far are fabricated using sophisticated deposition methods that are usually incompatible with large area processing and hence potentially expensive. Here, it is shown an alternative processing method based on spray pyrolysis and soluble precursor molecules for the deposition of both high- $k$   $\text{ZrO}_2$  and  $\text{Y}_2\text{O}_3$  oxide dielectrics and high-performance zinc oxide (ZnO) based semiconductors onto large area substrates under atmospheric conditions. Implementing  $\text{ZrO}_2$  and  $\text{Y}_2\text{O}_3$  as the gate dielectrics, ZnO-based TFTs were manufactured that are characterised by low voltage operation (4-6 V) hysteresis-free operation, field-effect mobilities exceeding  $30 \text{ cm}^2/\text{Vs}$  and channel current on/off modulation ratio in the range of  $10^5 - 10^6$ . The present results demonstrate that spray pyrolysis is a versatile tool for the deposition of oxide dielectrics and semiconductors onto large area substrates and provides a new route for the rapid development of materials far beyond those accessible by traditional deposition methods.

# Martensitic transformation and thermoelasticity in copper based shape memory alloys

O. Adiguzel

Firat University, Department of Physics  
23169 Elazig / Turkey

## ABSTRACT

Shape memory alloys are a new class of functional materials with a peculiar property known as shape memory effect. These alloys have an ability to recover a particular shape, and involve the repeated recovery of macroscopic shape of material at different temperatures. The functional behavior of shape memory alloys are based on the first-order martensitic transition. Copper based alloys exhibit this property in beta- phase field, which possess simple bcc-structures at high temperature austenite phase. As the temperature is lowered, austenite phase undergoes martensitic transition following two ordering reactions, and microstructural changes in microscopic scale govern this transition. The ordered parent phase structures turn into non-conventional layered structures by means of lattice invariant shears on a  $\{110\}$  - type plane of austenite matrix and these structures depend on the atom distribution at parent phase.

**Key Words:** Shape memory effect, martensite, thermoelasticity, atom sizes, layered structures, hexagonal distortion.

## 1. Introduction

Shape memory alloys take place in a class of functional materials by exhibiting a peculiar property called shape memory effect. This property is characterized by the recoverability of a certain shape of material at different conditions. These alloys involve the repeated recovery of macroscopic shape of material at different temperatures. This behavior is called thermo-elasticity, as well. The origin of this phenomenon lies in the fact that the material changes its internal crystalline structure with changing temperature. Shape memory effect is associated with martensitic transformation which is a solid state phase transformation occurring with the cooperative movements of atoms in the alloy on cooling from high temperature austenite phase region. Shape memory effect refers to the shape recovery of materials resulting from martensite to austenite transformation when heated above reverse transformation temperature after deforming in the martensitic phase. These alloys also cycle between two certain shapes with changing temperature. Copper based shape memory alloys exhibit this property in metastable  $\beta$ -phase field. High temperature  $\beta$ -phase bcc-structures martensitically undergo the non-conventional structures following two ordered reactions on cooling, and structural changes in nanoscale level govern this transition cooling [1-3].

In the shape memory alloys, the austenite lattice has a higher order of symmetry than that of martensite. More than one martensite variant can be induced from one austenite. Martensite variants have identical crystal lattice, but are oriented in different directions [4]. The martensitic transformation is a shear-dominant diffusionless solid-state phase transformation, and when a shape memory alloy undergoes a martensitic phase transformation, it transforms from the parent phase to one or more of the different variants of the martensitic phase [5, 6].

Martensitic transformations occur in a few steps. First one is Bain distortion based on lattice deformation mechanism. This mechanism can be described as follow: Starting from the long range order  $\beta$ -phase, an fct cell is delineated in matrix, and this cell undergoes to the corresponding fcc lattice with Bain distortion which consists of an expansion of 26% parallel to  $[001]_{\beta}$  axis and a compression of 11% normal to this axis as seen from Figure 1 .

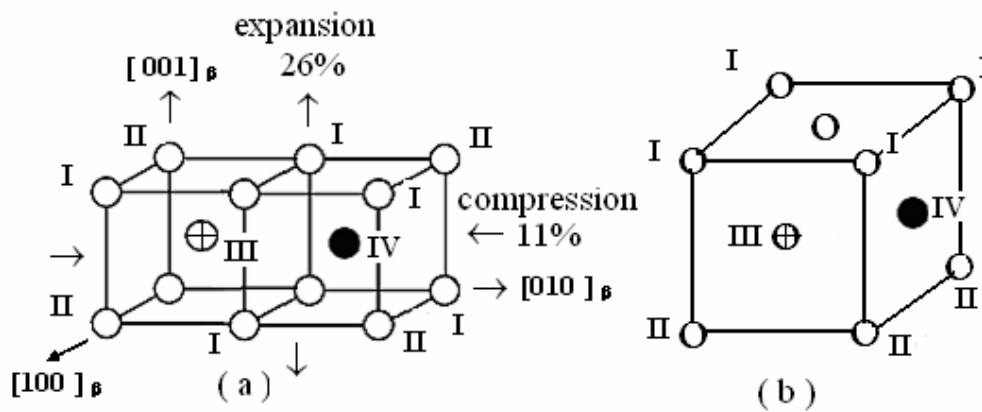


Figure 1. (a) Two bcc-unit cells (quarter of  $\text{Cu}_2\text{AlMn}$  ( $L2_1$ )- type unit cell) and sublattices I-IV, (b) martensitic fcc-structure formed by Bain distortion showing the inherited sublattice positions.

Second step is lattice invariant shear mechanism, which causes the cooperative movement of atoms less than interatomic distances on a  $\{110\}$  - type plane of austenite matrix which is basal plane of martensite. These shears give rise the formation of unusual complex structures called long period layered structures such as 3R, 9R or 18R depending on the stacking sequences on the close-packed planes of the ordered lattice. The complicated long-period stacking ordered structures mentioned above can be described by different unit cells. All of these martensite phases are long-period stacking ordered structures that is the underlying lattice is formed by stacks of close-packed planes. In case the parent phase has a B2-type superlattice, the stacking sequence is ABCBCACAB(9R) [2, 7]. The stacking of  $(110)_\beta$  - planes in  $\text{DO}_3$ -type structure and formation of layered structures are shown in Figure 2. Martensitic transformation is characterized by a change in the crystal structure of the material at the nano-level rather than micro-level, and the transformed region consists of parallel bands containing alternately two different variants. All of these martensite phases have the long-period stacking ordered structures, and microstructural evaluation provides a mechanism by which the transformation from the high temperature austenite phase to the low temperature martensite phase takes place.

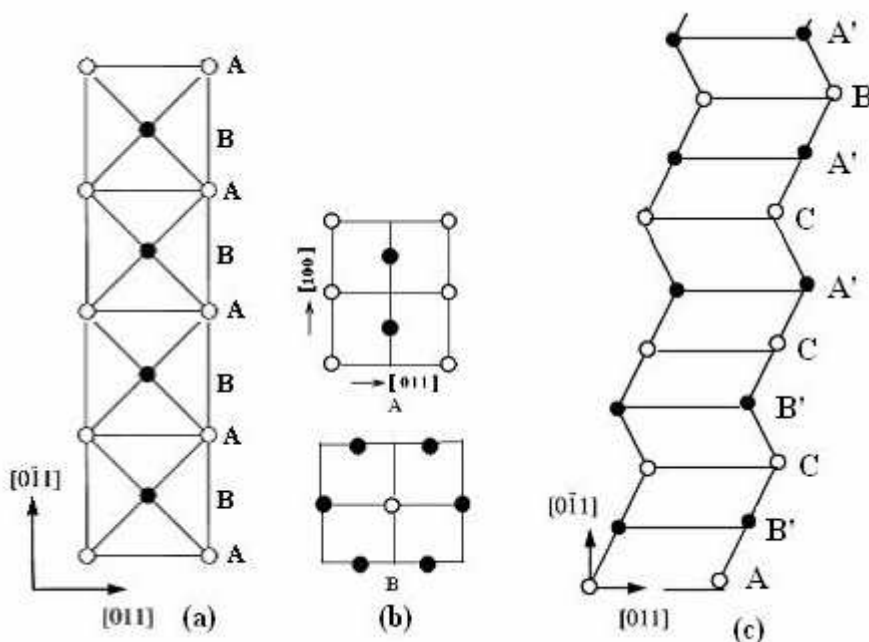


Figure 2: a) Stacking of  $(110)_\beta$  planes viewed from  $[001]_\beta$  direction in  $\text{DO}_3$ -type structures, b) atomic configuration on first and second layers of  $(110)_\beta$  plane in  $\text{DO}_3$ -type structures, c) inhomogeneous shear and formation of layered structures.

The fundamental structures of the beta-type martensites are orthorhombic close-packed structures, and monoclinic distortion takes place in some cases by means of microstructural evaluation depending on the atomic distribution in nanoscale or angstrom level, and 18R structure is modified as M18R.

## 2. Experimental

In the present contribution, two copper based ternary alloys were selected for investigation: a CuZnAl alloy with a nominal composition by weight of 26.1%zinc, 4%aluminium, the balance copper, while the other was a CuAlMn alloy with a nominal composition by weight of 11% aluminium, 6% manganese and the balance copper. Powder specimens for X-ray examination were prepared by filling the alloys. Specimens for TEM examination were also prepared from 3mm diameter discs and thinned down mechanically to 0.3mm thickness. These specimens were heated in evacuated quartz tubes in the  $\beta$ -phase field (15 minutes at 830°C for CuZnAl and 20 minutes at 700°C for CuAlMn) for homogenization and quenched in iced-brine. These specimens were also given different post-quench heat treatments and aged at room temperature.

TEM and X-ray diffraction studies carried out on these specimens. TEM specimens were examined in a JEOL 200CX electron microscope, and X-ray diffraction profiles were taken from the quenched specimens using Cu- $K_{\alpha}$  radiation with wavelength 1.5418 Å.

## 3. Results and Discussion

An x-ray powder diffractogram taken from the quenched CuZnAl alloy samples is shown in Figure 3. This diffractograms which exhibits superlattice reflection has been indexed on the monoclinic M18R basis. X-ray diffraction profile of CuAlMn alloy also exhibit similar configuration. Two electron diffraction patterns taken from CuZnAl alloy sample are also shown in Figure 4, respectively. X-ray powder diffractograms and electron diffraction patterns reveal that these alloys exhibit superlattice reflections. X-ray powder diffractograms and electron diffraction patterns taken from the specimens in a large time interval were compared with each other. It has been observed that electron diffraction patterns exhibit similar characteristics, but some changes have been occurred in the locations and intensities of diffraction peaks on the x-ray diffractograms with aging duration. It has been observed that some peak pairs come close each other with ageing duration[8]. These changes imply new transitions which have diffusive character. It means that some neighbor atoms change their locations.

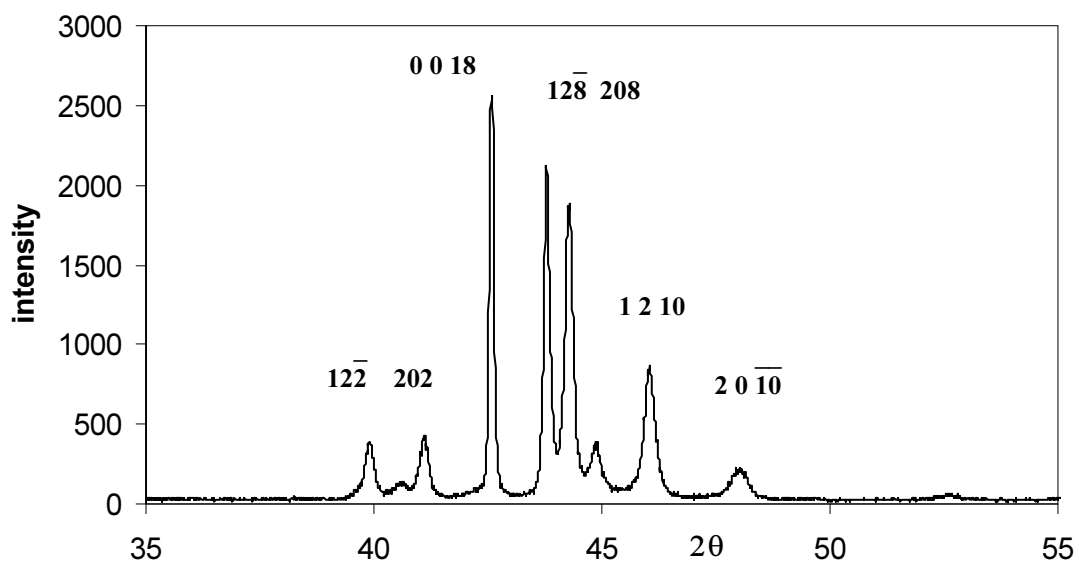


Figure 3: a) An x-ray diffractogram taken from the CuZnAl alloy sample.

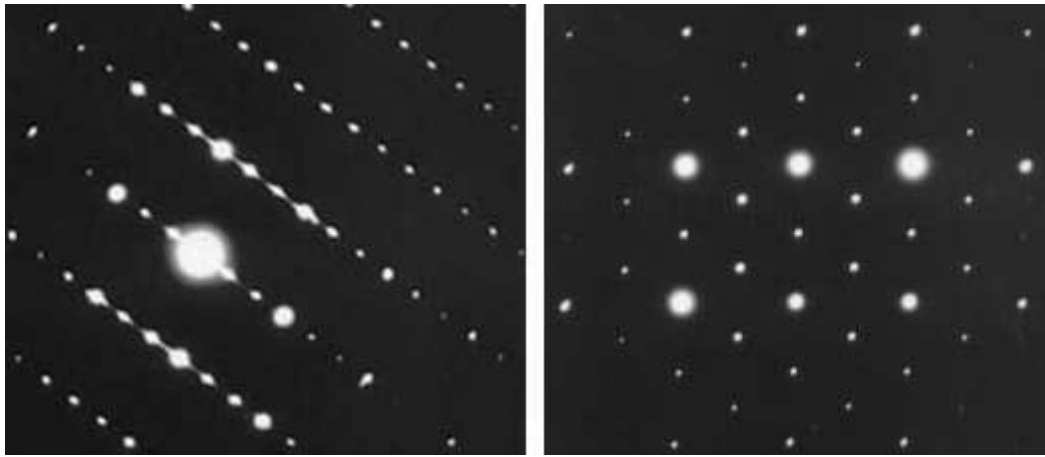


Figure 4: Electron diffraction patterns taken from CuZnAl and CuAlMn alloy samples.

It is interesting that miller indices of these plane pairs provide a special relation:  $(h_1^2 - h_2^2)/3 = (k_2^2 - k_1^2)/n$  where  $n=4$  for 18R martensite [1, 8]. These plane pairs can be listed as follow; (122)-(202), (128)-(208), (1 2 10) – (2 0 10), (040)- (320). This observation can be attributed to a relation between interplane distances of these plane pairs. In the disordered case, atom sizes can be taken nearly equal, and martensite basal plane becomes an ideal hexagon. Therefore, if the interplane distances are calculated, it can be seen that these values will be equal each other for the pairs and diffraction peaks overlap each other. In the ordered case, neighbour atom sizes are different, interplane distances become different and each peak appears separately [8]. On the other hand, the alloys have the layered complex structure in martensitic state. The monoclinic distortion of 18R-type structure contributes to the martensite stabilization which proceeds by a diffusion-controlled process [9]. Metastable phases of copper-based shape memory alloys are very sensitive to the ageing effects, and heat treatments can change the relative stability and the configurational order of crystal planes. The parent phase has highly symmetric structure and the product phase has internally twinned and complex structures.

Also, several types of microscopic deformation involving changes can occur in the stacking sequence of close-packed planes of material with martensite formation [2, 10]. This change gives rise the increase in the complexity of crystal structure.

Atom locations in the lattice sites in the crystal unit cell are very important for the analysis and process of transformation.

It can be concluded from the above results that the copper-based shape memory alloys are very sensitive to the ageing treatments, and heat treatments can change the relative stability and the configurational order of atoms in the material. This result attributes to rearrangement of atoms in diffusive manner.

## References

- [1] O. Adiguzel, *Materials Research Bulletin*, **30**, 755 (1995).
- [2] J. J. Zhu, K.M. Liew, *Acta Materialia*, **51**, 2443 (2003).
- [3] Y. Sutou *et al*, *Acta Materialia*, **53**, 4121 (2005).
- [4] R. D. James and K. F. Hane, *Acta Materialia*, **48**, 197 (2000).
- [5] K.Otsuka and T. Kakeshita, *MRS Bulletin*, **27**, 91 (2002).
- [6] P. Popov P and D.C. Lagoudas, *International Journal of Plasticity*, **23**,1679 (2007).
- [7] J.L. Pelegrina and R. Romero, *Materials Science and Engineering A*, **282**, 16 (2000).
- [8] O. Adiguzel, *Journal of Materials Processing Technology*, **185**, 120 (2007).
- [9] Z. Li, S. Gong, M. P. Wang, *Journal of Alloys and Compounds*, **452**, 307 (2008).
- [10] V. Paidar, *Materials Science and Engineering A*, **481–482**, 243 (2008).

## **Ab-initio thermodynamic calculations of substitutional impurities at planar defects in Aluminum**

**J.-M. Albina<sup>1\*</sup>, C. Elsaesser<sup>1,2</sup>, T. Gnielka<sup>2</sup>, and P. Gumbsch<sup>1,2</sup>**

<sup>1</sup>Fraunhofer Institute for Mechanics of Materials IWM, Wöhlerstr. 11, 79108 Freiburg, Germany

<sup>2</sup>IZBS, University of Karlsruhe, Kaiserstr. 12, 76131 Karlsruhe, Germany

\* jan-michael.albina@iwf.fraunhofer.de

First-principles electronic-structure calculations based on the density functional theory with the local density approximation (LDA) were carried out for investigating the energetic stability of segregated alloying elements at planar defects in aluminum.

Several simple and transition metals were selected as alloying elements and introduced as substitutional point defects in low concentration (less than 10 at.-%) at planar defects of face-centered cubic aluminum. Extrinsic and intrinsic stacking faults as well as several  $\Sigma 3$  grain boundaries were investigated.

We will present results for the formation energies of planar defects with point defects as a function of the alloying elements' species and concentration. We will discuss the strength and weaknesses of such approach to provide a practical and straightforward estimation for interface and segregation energies in alloys.

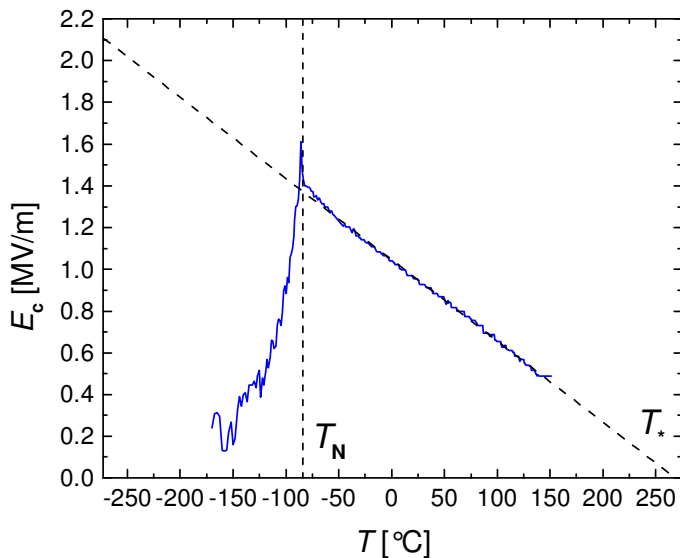
This work was supported by the Bundesministerium für Bildung und Forschung (BMBF-WING) "Virtual development of materials", grant No. 03X0511A-C.

# Creep in ferroelectric ceramics: mechanisms and modeling

A. YU. Belov<sup>1</sup>

<sup>1</sup>Institute of Crystallography RAS, Leninskii Prospect 59, Moscow, 119333 Russia  
e-mail: belov@crys.ras.ru

Creep in ferroelectric ceramics is a relatively slow change in polarization with time under constant external field. The main issue in the experimental analysis and theoretical modeling of creep consists in the separation of contributions of different mechanisms controlling the polarization reversal in ferroelectrics, namely, growth of the existing domains by the domain wall motion and nucleation of new domains [1]. Here, the temperature dependent ferroelectric hysteresis is used to probe both the activation field for domain nucleation and the pinning potential for the domain wall motion. It is shown that the parameters used in micromechanical models of creep can be directly assessed from the experimental data on the temperature dependence of the coercive field  $E_c(T)$ , see Figure 1 [2]. In particular, the peak  $T_N$  in the low-temperature region is related to the activation field, controlling the domain nucleation, and the temperature  $T_*$  provides information on the unpinning



activation energy, which characterizes the interaction between domain walls and obstacles. The micromechanical models based on both nucleation and pinning are developed and applied to creep modeling in soft PZT ferroelectric ceramics. The effects of internal fields on the activation energy of creep are incorporated within the framework of a mean-field approximation [1].

Figure 1. Experimental dependence of the coercive field  $E_c$  on temperature for commercial PZT ceramic PIC 151 at a frequency of 10 Hz and electric field amplitude of 2.0 MV/m [2]. Dashed lines illustrate the definition of the parameters  $T_N$  and  $T_*$ .

## References

1. A.Yu. Belov, W.S. Kreher, "Creep in soft PZT: the effect of internal fields", *Ferroelectrics* **391**, 12 (2009).
2. A.Yu. Belov, W.S. Kreher, M. Nicolai, "The evaluation of activation parameters for ferroelectric switching in soft PZT ceramics", *Ferroelectrics* **391**, 42 (2009).

# Performances of a Multifunctional Hollow Sphere-based Foam for Applications at High Temperature

**Cécile Davoine, Fabienne Popoff, Anaïs Götzfried**

ONERA Office National d'Études et de Recherches Aérospatiales  
Dept. Matériaux et Structures Métalliques  
BP72 - 29, avenue de la Division Leclerc  
FR-92322 Chatillon Cedex

Well-known advantages of cellular metals are their high ability for energy absorption, good damping behavior and sound absorption at a high specific stiffness. A process for making superalloy foams composed of brazed hollow spheres has been recently developed by ONERA [1]. From the structural point of view, the “closed cells” materials present greater resistance to the mechanical load than “open cells” materials. The compromise was to choose a “closed-open” cells material, having an open porosity for acoustic absorption and a closed porosity for mechanical load resistance. These multifunctional superalloy hollow sphere-based foams meet the demanding requirements of aerospace propulsion applications by offering acoustic absorption and high specific strength at room temperature. In order to find load-bearing and acoustic damping applications, e.g. as the core of sandwich structures in engines, performances of these foams need to be characterized at high temperature, in particular the influence of the oxidization phenomenon on the specific properties of the superalloy foams.

This work focuses on the evolution of mechanical and acoustic properties with oxidation. The oxidization kinetics of such an ultra-high porous metallic architecture was investigated in the temperature range of 800-1000°C during 1000 hours in air. The size of the pore channels and the tortuosity of open cells was observed by SEM to characterize the impact of the oxide film formation. The influence of the oxidation level on the acoustic properties of hollow sphere structures was studied. The absorption coefficient was analysed experimentally by an impedance tube in the frequency range of 800 - 4000 Hz. Results fit well to theoretical investigations described by the Lafarge-Pride analytical model. An experimental investigation of the quasi-static uniaxial compressive loading of the superalloy foam has been carried out. This study shows that this ductile metallic foam consisting of an oxidation-resistant alloy could find multi-fonctionnal applications at high temperature.

[1] C. Davoine, A. Götzfried, S. Mercier, F. Popoff, A. Rafray, M. Thomas, V. Marcadon, Metallic Hollow Sphere Structures Manufacturing Process, Mater. Res. Soc. Symp. Pro. Vol 1188 2009, p 89-94

**Finite size effects in oxide nanoparticles:  
On the origin of lattice expansion and contraction**

**Manuel Diehm<sup>1,2</sup>, Peter Agoston<sup>1</sup> and Karsten Albe<sup>1</sup>**

<sup>1</sup>Technische Universität Darmstadt, Institut für Materialwissenschaft,  
Petersenstraße 23, 64287 Darmstadt, Germany

<sup>2</sup>E-mail: mdiehm@mm.tu-darmstadt.de

The expansion of the crystal lattice with decreasing particle size has been reported for various oxide materials in the past decade. This effect likely plays a pivotal role for modifying the functional properties of nanoparticles. The effect itself, however, is scarcely understood. Three basic explanations have been suggested so far, namely expansive surface stresses, increased vacancy concentrations with a coupled valency reduction of the cations and finite size effects on the Madelung lattice sum.

In this contribution we systematically examine the fundamental reasons behind the lattice expansion, employing molecular statics simulations with ionic shell potentials and a novel dynamic charge-transfer bond-order potential. Moreover DFT calculations are used to confirm the principal results and enquire further into effects that can not be adequately modeled within the framework of classical potentials.

Our simulations reveal that both lattice expansion and lattice contraction can be observed, the behaviour depending on the material and potential model. It is shown under what conditions the finite size effect on the Madelung sum causes lattice expansion and how covalent effects can modify this behaviour. We further highlight the decisive role of surface stresses in determining the changes in the crystal lattice and point out possible mechanisms that cause the surface stress to become expansive. The Shuttleworth equation connecting surface energy and surface stress is confirmed to hold for all investigated materials and underlying interaction models.

## Multiscale Material Modelling for Li-Ion Batteries

**Thomas Eckl<sup>1</sup>, Esther Bohn<sup>1</sup>, Jake Christensen<sup>2</sup>, Marc Kamlah<sup>3</sup> and Robert McMeeking<sup>4</sup>**

<sup>1</sup>Robert Bosch GmbH, Corporate Sector Research and Advance Engineering,  
Applied Research 1 - Materials (CR/ARM1)  
Postfach 10 60 50, 70049 Stuttgart, Germany  
[thomas.eckl@de.bosch.com](mailto:thomas.eckl@de.bosch.com)

<sup>2</sup>Robert Bosch LLC, Palo Alto, CA, USA

<sup>3</sup>Karlsruhe Institute of Technology, Karlsruhe, Germany

<sup>4</sup>University of California Santa Barbara, Santa Barbara, CA, USA

During a typical charge/discharge cycle of a Li-ion battery the active intercalation materials experience a volume change of up to 10%. This causes fracturing and loss of contact of the active particles and finally the degradation of the whole cathode/anode. A careful understanding of these mechanical-electrochemical degradation mechanisms is mandatory to fulfil the high quality and lifetime requirements in automotive applications.

Here we present a new multiscale modelling approach for degradation of Li-ion batteries. The centre of our approach is a one-particle micromechanical diffusion model. The driving force for diffusion is deduced from basic thermodynamics and statistical physics and allows the modelling of phase-change materials. The arbitrarily shaped and positioned particles are then coupled to the pseudo two-dimensional electrochemical “dualfoil” battery-cell model. Various coupling schemes between our micromechanical particle model and the electrochemical battery-cell model, which couples the microstructure to the charge/discharge cycles of “real-world” battery applications, will be discussed.

The parameters of our one-particle micromechanical diffusion model can be directly obtained from ab-initio DFT calculations if they are experimentally not accessible or in cases where new computer-designed materials are to be evaluated.

Strengths and limitations of our multiscale modelling approach will be discussed thoroughly, in particular with focus on the needed experimental input. Finally, we discuss extensions of our model like many-particle microstructural models (including e.g. binder, conductive additives, etc.) and the explicit modelling of crack-growth.

## Multifunctional oxides - The influence of defects on the ferroic properties

S. Gemming<sup>1,\*</sup>, M. Zschornak<sup>1,2</sup>, T. Weißbach<sup>2,3</sup>, H. Stöcker<sup>2,3</sup>, D.C. Meyer<sup>2,3</sup>, T. Gemming<sup>2,4</sup>, A. Lubk<sup>2,5</sup>, N. A. Spaldin<sup>5</sup>

<sup>1</sup>FZ Dresden-Rossendorf, D-01314 Dresden, Germany.

<sup>2</sup>Institute of Physics, Technical University Dresden, D-01061 Dresden, Germany.

<sup>3</sup>Institute of Physics, TU-BA Freiberg, D-09596 Freiberg/Sachsen, Germany.

<sup>4</sup>IFW Dresden, P.O. Box 270116, D-01171 Dresden, Germany.

<sup>5</sup>Materials Department, U.C. Santa Barbara, California 93106-5050, USA.

\*Full address: Institute of Ion-Beam Physics and Materials Research, P.O. Box 51 01 19, FZ Dresden-Rossendorf, D-01314 Dresden, Germany; e-mail: s.gemming(at)fzd.de.

Transition metal oxides exhibit a wealth of physical phenomena, among them ferroic properties such as ferroelasticity, ferroelectricity and ferromagnetism, or their combination in multiferroics. In addition, transition metal oxides are sensitive to the chemical environment via the external partial pressure of oxygen; changes induce stoichiometry deviations, which cause conductivity changes and modify the ferroic characteristics.

The present study focuses on SrTiO<sub>3</sub>, YMnFeO<sub>5</sub>, and BiFeO<sub>3</sub> and correlates local changes due to point and planar defects with changes of the elastic, polarization and magnetic properties. The microscopic interactions are determined by density-functional calculations, which yield the basis for more large-scale simulations with effective Hamiltonian approaches.

Under oxygen-poor conditions oxygen vacancies in SrTiO<sub>3</sub> accumulate in an external electric field and reduce the hardness. In an Sr/O-rich environment the phases SrO(SrTiO<sub>3</sub>)<sub>n</sub> are formed, which yield a distinct change of the X-Ray reflectivity due to the regular arrangement of extrinsic SrO(001) stacking faults.

YMn<sub>2</sub>O<sub>5</sub> has a series of complex antiferromagnetic phases in coexistence with ferroelectricity. In YFeMnO<sub>5</sub>, only one commensurable ferrimagnetic phase was found and ferroelectricity is absent. Based on spin-polarized DFT calculations a Heisenberg model yields the coupling constants of the Fe-substituted and the manganese-only compounds and relates them to crystal-field interactions.

BiFeO<sub>3</sub> is a rhombohedral multiferroic with several domain wall configurations.

Among them, the 109° and 180° walls have a significant change in the component of their polarization perpendicular to the wall; the corresponding step in the electrostatic potential is consistent with a recent report of electrical conductivity at the domain walls. Changes in the Fe-O-Fe bond angles at the walls change the canting of the Fe magnetic moments which can enhance the local magnetization.

# First Principles Determination of Phase Transitions in Magnetic Shape Memory Alloys

**Tilmann Hickel, Ali Al-Zubi and Jörg Neugebauer**

Max-Planck-Institut für Eisenforschung GmbH, Max-Planck-Str. 1, 40237 Düsseldorf  
hickel@mpie.de

Martensitic phase transformations are of key importance for many modern material systems. They are responsible for high work-hardening rates and tensile strength in advanced steels as well as for the shape memory effect in various metallic alloys. A first principles determination of such first order structural transitions is often challenging, if different excitation mechanisms or a softening of vibrational modes needs to be considered. This applies also to  $\text{Ni}_2\text{MnGa}$ , being a typical Heusler alloy that shows a shape memory effect. In the high-temperature austenitic phase it has a cubic  $L2_1$  structure, whereas below a critical temperature the symmetry is reduced by an orthorhombic distortion with lattice deformations of up to 10%. Due to the ferromagnetic order, the transition between several orthorhombic variants can also be triggered by a magnetic field. The material system is therefore a very promising candidate for applications, but its operation temperatures and ductility still need to be improved. For this purpose an extension of the currently very limited knowledge on the phase diagram and the nature of the transitions is decisive.

In order to identify the stable structures and their transitions we performed ab initio calculations of free energies for the austenite, the (modulated) pre-martensite and the unmodulated martensite. Quasiharmonic phonons and fixed-spin magnons are considered, employing density functional theory. Particular care has been taken to determine the shuffling structures related to soft phonons. Using this approach we were able to successfully describe the phase transition in detail, to reveal the involved delicate interplay of vibrational and magnetic excitations and to accurately determine the transition temperature [1]. The methods developed for the Heusler systems can now be applied to predict structural phase transitions also in other materials.

## References

[1] M.A. Uijtewaal, T. Hickel, J. Neugebauer, M.E. Gruner, P. Entel, Phys. Rev. Lett. 102, 035702 (2009).

# Interface investigations of TiN with Si<sub>3</sub>N<sub>4</sub>, Si and Ti overlayers using AR-XPS

**Dominik Jaeger<sup>1</sup>, Jörg Patscheider<sup>2</sup> and Laszlo Forro<sup>3</sup>**

<sup>1</sup>[dominik.jaeger@empa.ch](mailto:dominik.jaeger@empa.ch), Empa, Überlandstrasse 129, 8600 Dübendorf, Switzerland

<sup>2</sup>[joerg.patscheider@empa.ch](mailto:joerg.patscheider@empa.ch), Überlandstrasse 129, 8600 Dübendorf, Switzerland

<sup>3</sup>[laszlo.forro@epfl.ch](mailto:laszlo.forro@epfl.ch), EPFL, IPMC/SB, Lausanne, Switzerland

## Introduction

Nanocomposite coatings derive their extraordinary properties from a complex interplay between the involved phases. The chemistry of the grain-matrix interface of nanocomposites can not be probed by analytical techniques. Therefore a two-dimensional layer model of TiN with different overlayers is used to investigate the chemical states at the interface by Angle Resolved X-Ray Photoelectron Spectroscopy (AR-XPS).

## Materials & Methods

Quasi oxygen-free (<0.5at%) single crystalline TiN layers are prepared by unbalanced magnetron sputtering. They are covered with a few monolayers of Si<sub>3</sub>N<sub>4</sub>, Si and Ti in order to study the interfaces of differently terminated surfaces by XPS. XPS measurements are compromised by overlapping of TiO<sub>x</sub> contributions with the shake-up signal used in this study. To prevent oxidation the samples are transferred *in situ* using a vacuum transfer device. AR-XPS is performed to distinguish between surface, interface and bulk signal.

## Results

Besides the spin-orbit split main peaks Ti2p<sub>3/2</sub> and Ti2p<sub>1/2</sub>, unscreened shake-up satellites are observed in the XPS data, and at lower kinetic energies also surface and bulk plasmons are visible. To properly identify these intensities a Tougaard back ground subtraction is used to account for the constraints imposed by quantum mechanics.

With AR-XPS the variation of contributions at different depths can be resolved; it can therefore be used to delineate the signal at the interface. It is shown that the interfaces with different overlayers have a different ratio of unscreened to screened photoemission peaks, indicating a different valence electron concentration at the interface (see Fig.1). This means that these interfaces are polarized to a different extent. The area ratio of the shake-up peaks and the main peaks correlates to the bandgap of the overlying material. The polarization is increasing with higher bandgaps of the overlayer, indicating an increase of the interface strength from Ti and Si to Si<sub>3</sub>N<sub>4</sub>.

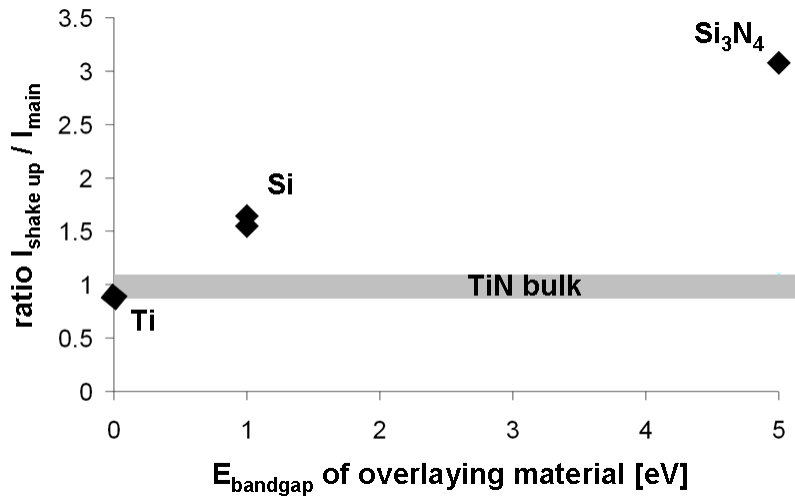


Fig. 1: Intensity ratio of the Ti2p satellite to main peak for overlayers with different bandgaps.

# Electronic structure and transport properties of transition-metal/SrTiO<sub>3</sub>(100) heterojunctions

E. M. Kalivoda, M. Mrovec, C. Elsässer

Fraunhofer Institute for Mechanics of Materials IWM, Wöhlerstraße 11, 79108  
Freiburg, Germany

## ABSTRACT

First-principles electronic-structure calculations based on the density functional theory and by means of the mixed-basis pseudopotential method were carried out for transition-metal/SrTiO<sub>3</sub>(100) heterojunctions. To analyze the influence of the metal on the leakage properties, Schottky barrier heights for the metal/SrTiO<sub>3</sub> interfaces were calculated by a step-by-step procedure that dissects the process of interface formation and enables one to distinguish between structural and electronic influences. We present results for a series of symmetrical metal/SrTiO<sub>3</sub>/metal sandwich structures and discuss the most relevant quantities that determine the band line-up at the interface.

## 1. Introduction

Perovskite oxides have attracted increasing interest in science and technology as potential alternatives to various silicon-based microelectronic components, for instance as dielectrics in thin-film capacitors or field-effect devices. In recent years much work has focused on strontium titanate (STO) and barium strontium titanate (BST) that are considered as representative perovskite oxides.

One of the crucial characteristics for the quality and reliability of integrated capacitors as well as field-effect devices is the leakage current. For the present nanometer-scale devices the leakage current is primarily affected by the atomic and electronic structure at the electrode/dielectric interface. Whereas experimental characterization at such small dimensions is usually difficult, theoretical first-principles density-functional-theory (DFT) studies can provide detailed and predictive insights into relationships of interfacial structures and electronic properties.

Since the perovskite oxides are insulating materials with a relatively small band gap (typically around 3.5 eV), the thermionic emission of electrons into band states is considered as one of the primary sources of leakage in thin perovskite films. The magnitude of the leakage current depends on the potential barrier at the interface between the insulating film and the metal electrode. This barrier, known as the Schottky barrier (SB), arises due to formation of the electron energy band offsets across the interface.

This work extends our previous work [1], where a systematic theoretical study of SBs was performed for a series of transition-metal(TM)/STO interfaces. While in our original study only monolayer TM coverages were considered, in the following we present an extension for thicker electrodes.

## 2. Method

The SB heights (SBH) were calculated by means of the mixed-basis pseudopotential (MBPP) approach of the DFT [2, 3, 4]. The local density approximation (LDA) was used for exchange and correlation [5, 6]. A discrete sampling with  $8 \times 8 \times 1$  k-points was used for Brillouin-zone

integration in total energy calculations. Computational details and a more extensive description of the MBPP-method are described in Ref. [1]. In the calculations of the TM/STO/TM heterojunctions we used supercell models with nine layers of STO and three layers of the TM embedded in a vacuum region. Since atomic rearrangements have a strong influence on the electronic structure, all supercell models were relaxed with forces on all atoms to be smaller than 0.01 eV/Å.

### 3. Results and Discussion

The formation of interfaces between transition metals and perovskite oxides involves a creation of new chemical bonds and substantial rearrangements of the electron density. Additionally, the bulk atomic positions in the vicinity of the interface are significantly altered to minimize the total energy of the system. Both of these processes contribute to the alignment of the energy levels at the interface and to the final charge distribution, which is associated with the formation of the depletion region, mostly on the side of the perovskite (see e.g. [7] and [8]).

In order to analyze these two processes independently, we followed the step-by-step procedure that was proposed in Ref. [1]. Within this analysis the total SBH for the electrons, the  $p$ -type SBH  $\Phi_{B,p}$ , can be expressed as a sum of three contributions:

$$\Phi_{B,p} = \Phi_{B,p}^{(0)} + \Delta\Phi_{B,p}^{(1)} + \Delta\Phi_{B,p}^{(2)}. \quad (1)$$

The first term on the right hand side  $\Phi_{B,p}^{(0)}$  is the ideal SBH in the Schottky-Mott limit [9], where no interactions between the materials at the interface are assumed. It is equal to the difference between the ionization potential (IP)  $I_S$  of STO, and the work function (WF)  $\Phi_{M,\text{bulk}}$  of the TM electrode:

$$\Phi_{B,p}^{(0)} = I_S - \Phi_{M,\text{bulk}}. \quad (2)$$

These two terms are related to the position of the valence band maximum of the STO and the Fermi energy of the TM, respectively. The last two terms in Eqn. (2) correspond to changes of the SBH due to atomic ( $\Delta\Phi_{B,p}^{(1)}$ ) and electronic ( $\Delta\Phi_{B,p}^{(2)}$ ) rearrangements [1]. Because the WF remains nearly unchanged when the atomic structure of metal surface changes to the interfacial atomic structure,  $\Delta\Phi_{B,p}^{(1)}$  equals to the change of the IP of STO,

$$\Delta\Phi_{B,p}^{(1)} = \Delta I_S^{(1)}, \quad (3)$$

which is related solely to the modification in the STO surface dipole. The second correction term  $\Delta\Phi_{B,p}^{(2)}$  is due to redistribution of the electron charge upon interface formation, which is necessary for the equalization of the Fermi level in the whole system. This process results in the transfer of electrons across the interface and thus leads to the creation of an interfacial dipole, which induces a step  $\Delta V^{(2)}$  in the electrostatic potential. The metal WF is again not changing. Hence the second correction term of the SBH equals to

$$\Delta\Phi_{B,p}^{(2)} = \Delta V^{(2)}. \quad (4)$$

The four contributions to the total SBH in Eqn. (2)-(4) are plotted in Fig. 1. The triangles correspond to the characteristic property of the metal electrode – the bulk WF  $\Phi_{M,\text{bulk}}$ . The stacked bars represent the evolution of the second key parameter – the position of the STO valence band. The reference level is the horizontal base line, which represents the IP  $I_S$  of the corresponding relaxed STO surface. For the nine-layer STO slab it is located at 4.14 eV and 6.57 eV below the vacuum level for the SrO and the TiO<sub>2</sub> terminations, respectively. The difference between the

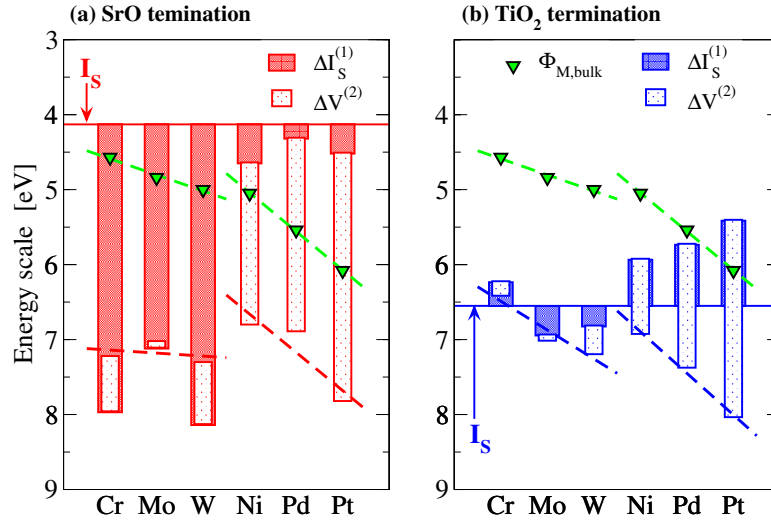


Figure 1: Different contributions to the SBH for the TM/STO/TM-junctions

base line (IP) and the triangles (WF) equals to the ideal SBH  $\Phi_{B,p}^{(0)}$  (see Eqn. (2)). The heights of the filled and empty bars then correspond to the shifts of the STO valence band due to atomic ( $\Delta I_S^{(1)}$ ) and electronic ( $\Delta V^{(2)}$ ) rearrangements, respectively. Finally, the resulting total values of the SBH  $\Phi_{B,p}$ , Eqn. (1), are listed in Tab. 1 together with the results from analysis of the local density of states (LDOS) of the oxygen atom in the central STO layer. These values were obtained by simply extracting the difference between the valence band maximum and the Fermi level.

Table 1: Total values of the SBH  $\Phi_{B,p}$  (in eV), determined by the step-by-step procedure – Eqn. (1) – and the LDOS-method.

	(a) SrO termination						(b) TiO <sub>2</sub> termination					
	Cr	Mo	W	Ni	Pd	Pt	Cr	Mo	W	Ni	Pd	Pt
Eqn. (1)	2.65	2.18	2.30	1.75	1.35	1.74	1.85	2.17	2.19	2.53	1.84	1.96
LDOS	2.45	2.36	2.48	1.87	1.39	1.79	1.89	2.08	2.05	1.90	1.76	1.88

As expected from the results of the systems with the TM monolayer [1], Fig. 1 reveals a very good correlation between the sum  $I_S + \Delta I_S^{(1)} + \Delta V^{(2)}$  and the metal WF for interfaces with the same termination and the same TM group. Tab. 1 shows a good agreement of the resulting SBHs (within 0.1 eV) between the two methods throughout the whole series. The only exceptions are the metals Cr, Mo, and W. In order to find out the cause of this deviation, we performed a detailed analysis of the Mo system. We repeated the SBH calculations with a thinner (7-layer) and thicker (11-layer) STO slab. These additional calculations demonstrate that the individual contributions to the SBH vary significantly with STO thickness, especially for the SrO-terminated STO. More specifically, with increasing STO thickness the contribution due to the change of the STO surface dipole upon atomic rearrangement becomes larger, while the change of the dipole during electronic rearrangement becomes smaller or even negative. A thorough analysis of the Mo system reveals that the surface dipole of the STO slab affects the atomic structure very far from the interface. The film thickness of nine or even eleven STO layers is therefore not yet sufficient for a fully converged result.

Interestingly, even though the individual contributions vary up to 1 eV, the total SBHs differ by only about 0.2 eV for STO slabs with different thicknesses. Thus, the results of the nine-layers system allow a reliable qualitative analysis and can serve as a basis for further discussions.

#### 4. Conclusion and Outlook

Our results confirm that the interface band alignment depends sensitively on the interface structure and chemistry imposed by the TM electrode. The step-by-step procedure for the determination of the SBH presents a reliable method, which enables a precise analysis of the contributing mechanisms, that are responsible for the SB formation. The present work serves as basis for future studies of electronic transport across the heterostructures when external bias is applied by shifting the Fermi energy of the metal electrodes relative to each other. These calculations will employ a nonequilibrium Green's function method, which provides the possibility to analyze the dependence of the electron transport properties on the applied bias.

#### Acknowledgements

Financial support for this work was provided by the German Research Foundation (DFG) through Project No. EL 155/17-2 in priority program 1157 "Integrated electroceramic functional structures" (M.M.), and Project No. EL 155/22-1 (E.M.K.).

#### References

- [1] M. Mrovec, J.-M. Albina, B. Meyer and C. Elsässer. Schottky barriers at transition-metal/SrTiO<sub>3</sub>(001) interfaces. *Phys. Rev. B*, **79**, 245121, 2009.
- [2] C. Elsässer, N. Takeuchi, K. M. Ho, C. T. Chan, P. Braun and M. Fähnle. Relativistic effects on ground state properties of 4d and 5d transition metals. *J. Phys.: Condens. Matter*, **2**, 4371, 1990.
- [3] K. M. Ho, C. Elsässer, C. T. Chan and M. Fähnle. First-principles pseudopotential calculations for hydrogen in 4d transition metals: I. Mixed-basis pseudopotential method for total energies and forces. *J. Phys.: Condens. Matter*, **4**, 5189, 1992.
- [4] B. Meyer, C. Elsässer, F. Lechermann and M. Fähnle. Fortran90 Program for Mixed-Basis Pseudopotential Calculations for Crystals. *Max-Planck-Institut für Metallforschung Stuttgart*.
- [5] D. M. Ceperley and B. J. Alder. Ground state of the Electron Gas by a Stochastic Method. *Phys. Rev. Lett.*, **45**, 566, 1980.
- [6] J. P. Perdew and A. Zunger. Self-interaction correction to density-functional approximations for many-body systems. *Phys. Rev. B*, **23**, 5048, 1981.
- [7] A. P. Sutton and R. W. Balluffi. Interfaces in Crystalline Materials. *Oxford University Press Inc.*, New York, 1995.
- [8] W. A. Harrison. Elementary Electronic Structure – Revised Edition. *World Scientific Publishing Co.Pte.Ltd.*, Singapore, 2004.
- [9] R. T. Tung. Recent advances in Schottky barrier concepts. *Mater. Sci. Eng.*, R. **35**, 1, 2001.

## A Bond-Order Potential for Silicon Carbide

**P.J. Kamenski<sup>1</sup>, M. Reese<sup>2,3</sup>, M. Mrovec<sup>2,3</sup>, C. Elsässer<sup>2,3</sup>, A.N. Kolmogorov<sup>4</sup>,  
R. Drautz<sup>5</sup> and D.G. Pettifor<sup>4</sup>**

<sup>1</sup> Department of Materials, University of Oxford, Parks Road, Oxford OX1 3PH, United Kingdom. email: [paul.kamenski@materials.ox.ac.uk](mailto:paul.kamenski@materials.ox.ac.uk)

<sup>2</sup> Fraunhofer-Institut für Werkstoffmechanik IWM, Wöhlerstraße 13, D-79108 Freiburg, Germany

<sup>3</sup> IZBS, Karlsruhe Institute of Technology, Kaiserstr. 12, 76131 Karlsruhe, Germany

<sup>4</sup> Department of Materials, University of Oxford, Parks Road, Oxford OX1 3PH, United Kingdom

<sup>5</sup> Ruhr-Universität Bochum, UHW 11/1112, Stiepel Str. 129, 44801 Bochum, Germany

Analytic bond-order potentials (BOPs) have been developed for carbon, silicon, and silicon carbide for use in large scale molecular dynamics simulations, such as modelling the growth of SiC nanocoatings. The analytic BOP parameters originate from orthogonal tight binding parameters, which are extracted from Density Functional Theory results. The analytic BOPs include up to fourth-moment interactions to capture the structural trends from the underlying tight binding model. We compare the results from Density Functional Theory, tight binding, and the analytic BOPs to show changes in observables, such as binding energies and defect energies, as tests of the analytic BOPs' accuracy. Resultant  $\sigma$  and  $\pi$  bond orders from the analytic BOPs are discussed, addressing the model's ability to describe bonding around point defects and surfaces. The usefulness of these analytic BOPs is assessed through comparison with the performance of other common interatomic potentials including the Tersoff [1], Erhart and Albe [2], and Vashishta [3] potentials.

### References:

[1] Tersoff, J., Modeling solid-state chemistry: Interatomic potentials for multicomponent systems. *Physical Review B*, 1989. 39(8): p. 5566.

[2] Erhart, P. and K. Albe, Analytical potential for atomistic simulations of silicon, carbon, and silicon carbide. *Physical Review B*, 2005. 71(3): p. 035211.

[3] Vashishta, P., et al., Interaction potential for silicon carbide: A molecular dynamics study of elastic constants and vibrational density of states for crystalline and amorphous silicon carbide. *Journal of Applied Physics*, 2007. 101(10): p. 103515-12.

# Anomalous Spin Transport in Magnetic Tunnel Junctions and Graphene Nanopatches

**N. Kioussis<sup>1</sup>, H. Y. Tang, A. Kalitsov<sup>2</sup>, W. H. Butler<sup>3</sup>, and Roberto Car<sup>4</sup>**

<sup>1</sup>Department of Physics, California State University Northridge, CA, U.S.A 91330-8236

E-mail: [.kioussis@csun.edu](mailto:.kioussis@csun.edu)

<sup>2</sup>SPINTEC, URA 2512 CEA/CNRS/INAC, Grenoble, France

<sup>3</sup>MINT Center, University of Alabama, Tuscaloosa, Alabama, USA

<sup>4</sup>Department of Chemistry, Princeton University, New Jersey, U.S.A 08544-0001

The current-induced magnetization reversal in magnetic tunnel junctions (MTJ) via the so called spin transfer torque has attracted intensive investigations both experimentally and theoretically. The bias behavior of the field-like,  $T_{\perp}$ , component of the spin torque directly related to the non-equilibrium interlayer exchange coupling (IEC), remains unresolved and controversial. I will present predictive results which show an oscillatory bias behavior of the field-like spin torque,  $T_{\perp}$ , in MTJ, which can be selectively controlled via the asymmetry in band filling between the ferromagnetic leads. This can lead to a linear or quadratic low-bias behavior, including tuning the bias-induced reversal of  $T_{\perp}$ . These findings reconcile the apparently contradictory experimental results recently reported in the literature. The underlying mechanism for the *non-equilibrium* IEC of non-collinear configurations is the interplay of four independent IEC for the majority- and minority-spin bands of the leads solely in the ferromagnetic (FM) configuration. I will also discuss the effect of disorder in the barrier on the bias behavior of  $T_{\perp}$ , and of the spin transfer,  $T_{\parallel}$ , components of the spin torque. The results reveal that the impurity-induced resonance states within the gap can be selectively tuned via the external bias and impurity energy level, changing in turn dramatically the bias behavior of both spin components. Finally, I will present recent predictions of the charge and spin transport in novel tunnel junctions comprising of zigzag-terminated graphene flakes connected to reconstructed zigzag-terminated graphene ribbons. For isolated graphene nanoflakes, we find novel electric-field induced transitions from antiferromagnetic to FM to non-magnetic states with increasing gate voltage, which can be used for switching unit devices. Pair of nanoflakes are found to exhibit giant tunnel magnetoresistance which can be used for engineering spin-transport applications.

# Modeling materials with optimized transport properties

Peter Kratzer,<sup>1</sup> Vladimir M. Fomin,<sup>1,2</sup> B. Hülsen<sup>3</sup> and M. Scheffler<sup>3</sup>

<sup>1</sup>Faculty of Physics, University Duisburg-Essen, Lotharstr. 1, 47048 Duisburg, Germany  
e-mail: Peter.Kratzer@uni-duisburg-essen.de

<sup>2</sup>Institute for Integrative Nanosciences, IFW Dresden, 01069 Dresden, Germany

<sup>3</sup>Fritz-Haber-Institut der Max-Planck-Gesellschaft, 14195 Berlin, Germany

## ABSTRACT

Following demands for materials with peculiar transport properties, e.g. in magnetoelectronics or thermoelectrics, there is a need for materials modeling at the quantum-mechanical level. We combine density-functional with various scale-bridging tools to establish correlations between the macroscopic properties and the atomic structure of materials. For examples, magnetic memory devices exploiting the tunneling magnetoresistance (TMR) effect depend crucially on the spin polarization of the electrodes. Heusler alloys, e.g.  $\text{Co}_2\text{MnSi}$ , if perfectly ordered, are ferromagnetic half-metals with (ideally) 100% spin polarization. Their performance as electrodes in TMR devices is limited by atomic disorder and deviations from perfect stoichiometry, but also by interface states at the tunneling barrier. We use *ab initio* thermodynamics in conjunction with the cluster expansion technique to show that excess manganese in the alloy and at the interface helps to preserve the desired half-metallic property. As another example, nanostructured materials with a reduced thermal conductivity but good electrical conductivity are sought for applications in thermoelectrics. Semiconductor heterostructures with a regular arrangement of nanoscale inclusions ('quantum dot superlattices') hold the promise of a high thermoelectric figure of merit. Our theoretical analysis reveals that an increased figure of merit is to be expected if the quantum dot size, the superlattice period and the doping level are all suitably fine-tuned. Such a superlattice thus constitutes a material whose transport properties are controlled by geometrical features at the nanoscale.

## 1. Introduction

Novel materials, in particular alloys or nanostructured materials, or heterostructures combining several materials into one, offer ample opportunities to find innovative solutions for devices with peculiar, tailored electrical transport properties. However, optimizing these materials or structures with respect to a particular figure of merit still poses a challenge to simulations: Because of the heterogeneity inherent in disordered alloys or in nanostructured samples, large systems, with possibly up to a hundreds of thousands of atoms, need to be modeled, and/or a huge configuration space needs to be explored. Moreover, it is crucial to consider quantum mechanics for electronic transport properties: Electronic states different from those known from the homogeneous bulk materials may arise due to the modification of the electronic band structure both by the local chemical environment in alloys and by the quantum confinement in nanostructures, or due to the quantum nature of electron tunneling through a potential barrier. Thus we need to use simulation tools that make use of information on the atomic and electronic scale, while at the same time taking into account varying materials properties, such as strain and composition fluctuations, on a much larger scale. In this paper, we will present examples of hierarchical multi-scale modeling that enables us to

combine information about the systems under study from different length scales, ranging from quantum effects on band structure and energy levels to macroscopic transport properties.

## 2. Formation energies, electronic and magnetic properties from a cluster expansion

Many systems relevant for electronic transport are crystalline in nature, i.e. the atoms are located on well-defined lattice positions, while displaying spatial inhomogeneities originating from various chemical species occupying the lattice sites, or from coherent nanoscale inclusions in an otherwise homogeneous host material. Retaining crystallinity is often crucial for achieving good electrical conductivity, because trapping of carriers or scattering due to defects usually severely limits the achievable conductivity in samples that are amorphous or have a poor crystallinity. In some of these crystalline systems, mechanical strain due to inhomogeneities is an important issue affecting the electronic structure, for example in semiconductor heterostructures with a lattice mismatch of the constituents. A possible way to treat these strain effects will be described further below. First, we will consider alloys where the local chemical environment of the constituent species is the dominant factor determining their electronic properties. Here, the cluster expansion technique can be helpful in tackling the complexity introduced by the huge number of possible atomic configurations that results from occupying each of the lattice sites randomly by one of the various species.

To give a specific example, we consider the Heusler alloy  $\text{Co}_2\text{MnSi}$  and its variants obtained by varying the relative concentrations of Co and Mn in this alloy. This material is of special interest, since density-functional theory calculations [1] predict the ideal  $\text{Co}_2\text{MnSi}$  alloy with the  $L2_1$  crystal structure to be a ferromagnetic half metal. This means that this material has electronic states at the Fermi level only in one spin channel, while displaying a band gap in the other spin channel. This makes  $\text{Co}_2\text{MnSi}$  attractive as material for spintronics, for example as electrode material in magnetic random-access memories that use the tunneling magneto-resistance (TMR) effect for the electronic read-out of the stored information. We are posing the question if the property of half-metallicity is stable when antisite defects, for example due to thermal disorder, are present, or when the relative concentration of Mn and Co in the alloy is varied.

The cluster expansion (CE) is a mathematical tool [2] that expresses a property of a system defined on a lattice by an expansion into an (in principle infinite) series of multi-site interactions, such as singles, pairs, triples, etc. This technique is useful, as one expects that, due to the 'near-sightedness' of nature, an expansion into a finite number of terms (a finite number of 'figures', as the building blocks of the expansion are called) will be sufficiently accurate for many systems and properties of interest. However, one should keep in mind that the validity of the series truncation needs to be checked carefully for each system and property one wants to investigate.

Since excellent reviews of the CE technique can be found in the literature [3], we only briefly explain the basic idea. Let us consider a binary alloy  $\text{A}_{1-x}\text{B}_x$  with  $N$  lattice sites. One particular configuration of the whole crystal is described by the occupation vector  $\boldsymbol{\sigma} = \{\sigma_1, \sigma_2, \dots, \sigma_N\}$ , where  $\sigma$  is +1 (−1) if a lattice point is occupied by atom A (B). For some property  $F$  of interest, e.g. the formation energy, the magnetic moment, etc., we may construct an expansion similar in structure to the Hamiltonian of the Ising model,

$$F(\boldsymbol{\sigma}) = J_0 + \sum_i J_i \sigma_i + \sum_{i,j} J_{ij} \sigma_i \sigma_j + \sum_{i,j,k} J_{ijk} \sigma_i \sigma_j \sigma_k + \dots,$$

where the pairs, triplets and higher order terms are the 'figures' of the CE. The effective cluster interactions  $J_i$  of the CE are determined from the results of a relatively small number of configurations ( $\approx 50$ ) obtained through first-principles computations. This can be achieved by a least-square fit of the predicted and the calculated values of  $F(\sigma)$  on subsets of the structures calculated within DFT [4]. Since in practice one is working with a truncated expansion with a finite number of 'figures', it is essential to check the transferability of the fit to other (unknown) configurations. A quantitative indicator of transferability is the cross-validation score, i.e. the average mean-square deviations on subsets for which DFT data are available, but have not been included in the fit in the first place. The set of figures that minimizes the cross-validation score is termed the optimal cluster expansion.

Once an optimum cluster expansion has been set up, the CE is a computationally inexpensive tool to explore the properties for a large number of configurations. A frequently studied property is the formation energy of alloys. There, the cluster expansion is useful in identifying ordered intermetallic compounds with a large supercell. In contrast to other computationally cheap simulation tools suitable to a large number of atoms, e.g. molecular dynamics using classical interatomic potentials, the cluster expansion may be used to represent also properties of quantum-mechanical origin directly in a simple and efficient way. For instance, a cluster expansion has been employed to search for configurations with high Curie temperature in the dilute magnetic semiconductor Ga(Mn)As [5]. Previously, this technique has also been used for finding semiconductor heterostructures with a prescribed band gap for given chemical constituents of the material [6]. More recently, we investigated the role of composition fluctuations in  $\text{CuIn}_x\text{Ga}_{1-x}\text{Se}_2$  for the local variations of the band gap in solar cells [7] using the CE method.

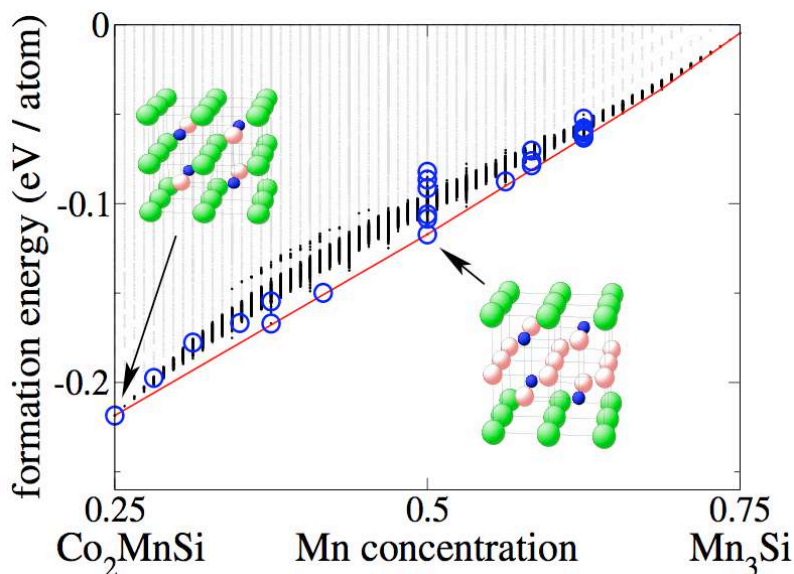


Figure 1. Formation energies of 27 million structures obtained from the cluster expansion by direct enumeration (light grey points). For the black points, the cluster expansion of the magnetic moments predicts an integer value. Both the integer magnetic moment and the existence of a spin gap has been confirmed by DFT calculations for the structures indicated by the circles.

In our present case of the Heusler alloy  $\text{Co}_2\text{MnSi}$ , we use a cluster expansion of the magnetic moment of the supercell [8]. Since a magnetic half-metal has an integer magnetic moment (an integer number of electrons in the minority spin channel that displays the energy gap), the magnetic moment serves as a necessary (although not sufficient) indicator of alloy compositions that possibly show half-metallicity. We find that the exchange of Co by Mn

atoms in the alloy most likely preserves the half-metallic property in a range of compositions. This is concluded from the results shown in Fig. 1, where the light gray data points indicate the formation energies of 27 million different configurations screened by the cluster expansion, while the black data points indicate those configurations for which the cluster expansion predicts an integer magnetic moment. It is remarkable that the region of black points has a certain width on the energy scale, indicating that even a configuration different from the ground state, that could result from a thermally excited atomic configuration or from imperfect annealing of the sample, might still preserve the half-metallicity for some Mn-enriched Heusler alloys. Since the integer magnetic moment is just a first indicator of half-metallicity, additional DFT calculations have been performed to test some selected configurations (circles in Fig. 1). Indeed an energy gap in the Kohn-Sham eigenvalue spectra of the minority spin channel has been found in all cases. In summary, Fig. 1 establishes that adding more Mn in the synthesis of  $\text{Co}_{2-x}\text{Mn}_{1+x}\text{Si}$  may even enhance its half-metallic properties. The robustness of Mn-enriched  $\text{Co}_2\text{MnSi}$  alloys for spintronics applications has been confirmed in a recent experimental study [9].

#### 4. Tunneling conductivity

One important application of half-metallic Heusler compounds is in TMR elements where two magnetic electrodes are separated by a very thin (only a few nanometer thick) oxide barrier. The relative magnetization of both electrodes is used to represent the bit of information stored in the TMR element, while the electrical conductivity of the tunnel junction serves as the read-out signal. The figure of merit is the TMR ratio, i.e. the difference of the conductance through the TMR device in the two states where the electrodes are magnetized either parallel or antiparallel to each other, divided by the smaller of the two values. Controlling the half-metallicity in the bulk of the electrodes by suitable alloy composition and materials processing (deposition and tempering steps) is prerequisite for achieving a high figure of merit. However, electronic states inside the gap in the minority spin channel at the interface between electrode and oxide barrier could act as centers for spin-flip scattering and could thus significantly diminish the figure of merit. In order to control and possibly eliminate this detrimental effect, one needs to know whether these interface states are localized at only one side of the oxide barrier (in the case of antiparallel magnetization of the electrodes), or if they extend through the barrier, and how much they contribute to the transmission of electrical current. The electronic properties of the interface states depend on their energetic position relative to the Fermi energy in the electrodes and on their orbital symmetry. The latter aspect is important for epitaxial, highly crystalline barriers made of MgO: An *s*-like character of the interface state allows for hybridization between the transition metal orbitals and the states derived from the conduction band in MgO, leading to metal-induced gap states, while a *3d*-like character of these states prevents their hybridization with any states near the fundamental band gap in the MgO. Which of these alternatives is realized is a question that can be answered by DFT calculations of the interface electronic structure.

Of course, the results of such calculations depend on the atomic structure of the interface. First, the energetically most favorable interface structure needs to be determined. Depending on the conditions under which the Heusler electrodes are prepared, i.e., if there is a surplus of Co or Mn, we find that the alloy will be terminated at the interface either by a Co layer (Co-rich conditions) or by a mixed MnSi layer (Co-poor conditions) [10]. Calculation of the Kohn-Sham band structure shows that electronic interface states in the minority spin channel occur for both of these terminations. An example is shown in Fig. 2 for the interface layer of Co atoms bonding to the oxygen atoms in the top-most MgO layer. However, the electrons in this state must tunnel through the MgO barrier with a finite crystal momentum parallel to the

interface, because the interface band crosses the Fermi level amid the  $\Gamma$ M and  $\Gamma$ X lines in the Brillouin zone (see Fig. 2, left panel). Moreover, the interface state has mostly Co-3d-orbital character. For both reasons, the wavefunction amplitude of the interface state is suppressed inside the MgO barrier (Fig. 2, right panel). Only if the Co<sub>2</sub>MnSi electrode is terminated by a full Mn layer, which is not stable in thermodynamic equilibrium, we find that the gap remains free of interface states.

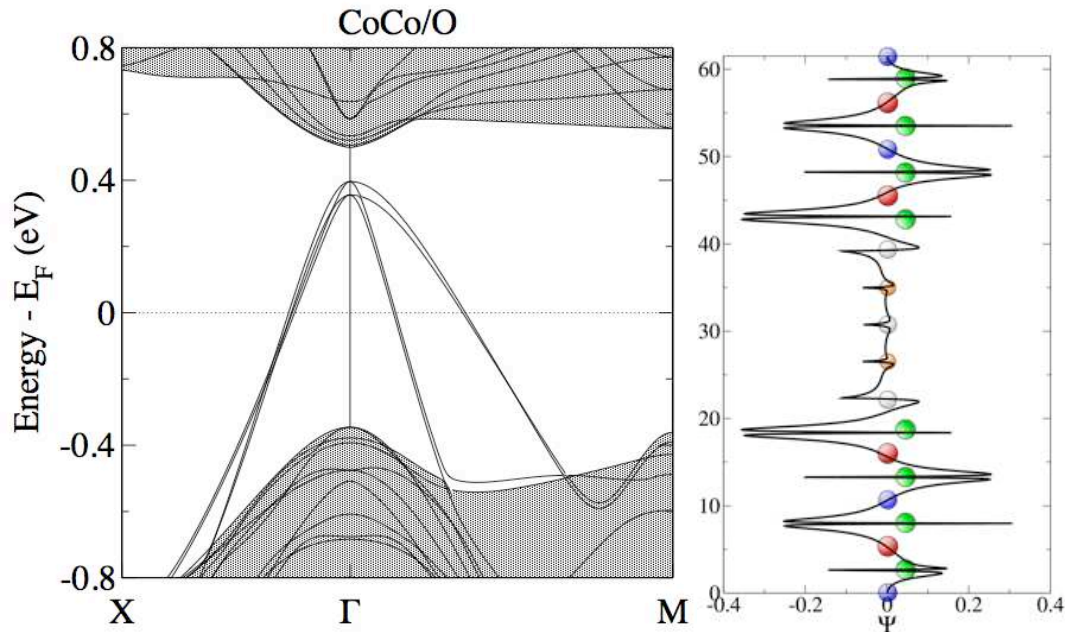


Figure 2. Kohn-Sham band structure projected onto the Brillouin zone of the interface in a Co<sub>2</sub>MnSi(001)/MgO(001)/Co<sub>2</sub>MnSi(001) heterostructure terminated by Co layers. The gap region in the minority spin channel is shown. The shaded regions correspond to projected bulk bands of Co<sub>2</sub>MnSi. The highly dispersive bands inside the gap are Co-induced interface states. The right panel shows the wavefunction belonging to the interface band at  $E_F$ . The vertical axis is a spatial coordinate normal of the interface. The small balls in the middle of the picture symbolize the Mg and O atoms of the barrier.

#### 4. Miniband transport in nanostructured materials

While tunneling conductance may be considered a quite special case, understanding the conductivity of a material in general not only requires knowledge about its electronic structure, but also about the mechanisms of energy and momentum relaxation, e.g. scattering of carriers by phonons and/or impurities. A truly first-principles modeling of the electric transport properties of real materials is therefore a very challenging task, and presently we can only present some steps towards a full theoretical treatment, with many steps left to future work. The first and mandatory step is always a quantum-mechanical modeling of the electronic structure, since ordered alloys or heterostructures may display electronic states substantially different from those of pure bulk materials, thus providing new channels for electronic transport.

Here, we present an example where nanostructuring a material has a pronounced effect on both its electronic structure and the mechanisms available for scattering of carriers: Semiconductors with a regular array of nanoscale inclusions coherent with the host lattice ('epitaxially self-assembled quantum dot crystals' [11]) display one-dimensional electronic minibands [12] that act as additional channels of conductivity. At the same time, we need to take into account that the electron-phonon scattering in these minibands is substantially

different from scattering in the bulk conduction band, mostly due the different phase space available for scattering in either case. In order to treat this complex, nanostructured system, we employ a multi-step approach [13]: First, atomistic modeling is used to describe the mechanical strain resulting from the nanoscale inclusions in the sample. The effect of the nanoscale confinement of the electrons in the quantum dots (QDs) and of the strain in both the quantum dots and the host matrix on the electronic structure is calculated quantum-mechanically from a tight-binding Hamiltonian. Thus, both the energetic position and the dispersion of the minibands are taken from a microscopic theory. On another level of modeling, for the calculation of the electron-phonon-scattering rate, we use a theory that is still state-specific, i.e. it calculates the scattering rate between quantum states with specific miniband index and crystal momentum, but uses a more coarse-grained input for evaluating the scattering matrix elements: The phonon dispersion is taken from an acoustic effective-medium theory, and the electronic wavefunctions are adopted from the analytic solution of a Kronig-Penney model of particles in a periodic array of quantum wells. The numerical value of the electron-phonon coupling strength is taken from experimental data. While all these pieces of information could in principle be obtained from the microscopic model as well, incorporating some level of empiricism allows us to perform the calculations faster and to explore systematically a variety of nanostructures differing in their geometrical parameters. Specifically, the simulations have been carried out for atomistic models of the structures shown schematically in Fig. 3. One supercell consists of about 50,000 atoms. The relaxation of the atomic positions is performed using an Abell-Tersoff-type force field [14]. The orthogonal tight-binding Hamiltonian builds on an  $sp^3s^*$  representation of the hopping matrix elements including first and second neighbors [15]. Spin-orbit coupling is included on an empirical level. The power-law dependence of the hopping matrix elements on interatomic distances [16] allows us to incorporate the effect of strain on the electronic states directly by setting up the Hamiltonian using the relaxed atomic positions. Periodic boundary conditions are employed to calculate Bloch states of the QD crystal. The folded-spectrum method is used to extract single eigenstates energetically located inside the band gap of the GaAs host, which physically correspond to the minibands in the QD stack.

#### 4. Nanostructured thermoelectrics

For applications in thermoelectric converters, one is interested in materials that maximize the dimensionless figure of merit  $ZT$ . It describes the maximum available electrical power for a given temperature gradient across the converter, and is defined as

$$ZT = \frac{\sigma S^2}{\kappa_{\text{el}} + \kappa_{\text{ph}}} T.$$

Here,  $\sigma$  is the electrical conductivity,  $S$  is the Seebeck coefficient,  $\kappa = \kappa_{\text{el}} + \kappa_{\text{ph}}$  is the thermal conductivity, comprised of an electronic contribution and a lattice contribution, and  $T$  is the absolute temperature. Optimally suited materials for thermoelectric applications should have a low thermal conductivity, but simultaneously a high electrical conductivity. These are requirements that are difficult to meet in bulk materials, where in many cases the electrical and the thermal conductivity (the electronic contribution thereof) are interrelated, e.g. by the Wiedemann-Franz law in metals. Obviously it is difficult to find a general strategy for optimizing  $ZT$ , but previous work suggests that materials with a narrow electronic band at the Fermi energy could allow one to achieve a high  $ZT$  value, both due to a high value of  $S$  in a narrow band, and a decoupling of  $\sigma$  and  $\kappa$  when scattering of carriers is only possible within a bandwidth smaller than  $k_{\text{B}}T$  [17,18]. Arrays of self-assembled semiconducting quantum dots

embedded in a semiconductor matrix are relevant in this context for several reasons: First, the nanoscale inclusions may act as very efficient scatterers of phonons with long and medium wavelength, thus suppressing thermal conductivity. For example, control of thermal conductivity down to  $< 1\text{W}/(\text{m K})$  range at the nanoscale via individual phonon scattering barriers has been recently achieved in multilayered Ge/Si QD arrays with as few as five barriers [19]. Secondly, one-dimensional electronic minibands for the motion perpendicular to the growth direction are formed if the spacer layers between subsequently grown layers of QDs are very thin, less than about ten nanometers. These narrow minibands open up the possibility to optimize the figure of merit [20], following the strategy outlined above.

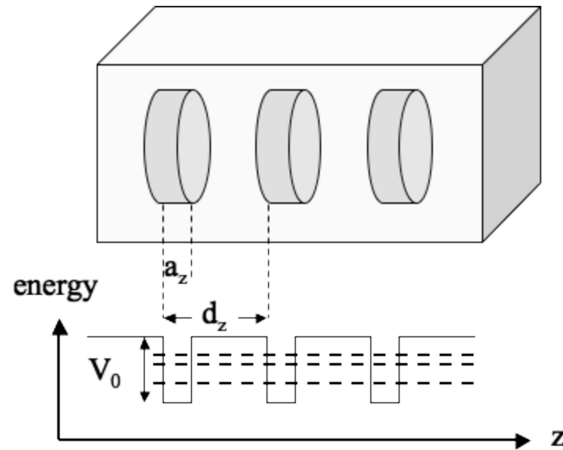


Figure 3. Schematic drawing of a stack of quantum dots of height  $a_z$ , with stacking period  $d_z$  (upper part). The sample was grown along the  $z$ -axis. The lower part schematically shows the periodic confining potential and the energetic position of the minibands (dashed horizontal lines).

In the following, we describe our search for optimal structural parameters of the QDs for the case of InAs QDs embedded in GaAs. We consider a one-dimensional stacking sequence, with period  $d_z$ , of QDs with height  $a_z$  (cf. Fig. 3). The parameter space of  $a_z$  and  $d_z$  has been explored in an attempt to optimize the figure of merit  $ZT$ , while the cylindrical shape of the QDs with a diameter of 10 nm has been kept for the sake of simplicity. As conceptual framework for calculating the transport coefficients  $\sigma$ ,  $S$  and  $\kappa_{\text{el}}$  entering  $ZT$ , we employ the semiclassical description of transport by the Boltzmann equation. Within each miniband, an energy-dependent carrier relaxation time  $\tau_J$  is used in solving Boltzmann's equation to first order in both the electric field  $E$  and the temperature gradient  $\nabla T$  by linear expansion around the equilibrium carrier distribution  $f_0$  :

$$v_{z,J}(k_z) \left[ eE + \frac{\varepsilon_J(k_z) - \mu}{T} \nabla T \right] \left( -\frac{\partial f_0}{\partial \varepsilon} \right) = \left( -\frac{\partial f_0}{\partial \varepsilon} \right)_{\text{coll}} \approx -\frac{f - f_0}{\tau_J(k_z)}.$$

We find that the carrier relaxation time, as calculated from Fermi's Golden Rule for the electron-acoustic-phonon scattering, displays significant structure inside the energy range of each miniband. Consequently, the approximation of a constant, energy-independent relaxation time, which is often made in calculating bulk conductivity, cannot be used for conductivity due to minibands. Within Boltzmann's theory, moments of the differential distribution function can be calculated,

$$L^{(\alpha)} = \sum_J \frac{2}{A} \int_0^{\pi/d_z} \frac{dk_z}{2\pi} \left( -\frac{\partial f_0}{\partial \varepsilon} \right) \tau_J(k_z) v_{z,J}^2(k_z) (\varepsilon_J(k_z) - \mu)^\alpha$$

and  $\sigma$ ,  $S$  and  $\kappa_{\text{el}}$  can be expressed in terms of these moments:

$$\begin{aligned} \sigma &= e^2 L^{(0)}, \\ S &= -\frac{1}{eT} \frac{L^{(1)}}{L^{(0)}}, \\ \kappa_{\text{el}} &= \frac{1}{T} \left( L^{(2)} - \frac{(L^{(1)})^2}{L^{(0)}} \right). \end{aligned}$$

The energy dispersion  $\varepsilon_J$  of the minibands and the pertaining group velocity  $v_{z,J}$  of the carriers entering the above equations are adopted from the tight-binding solution of an atomistic model of the QD stack.

To be able to make statements of practical relevance, it is necessary to extend our modeling by some more empirical elements: The carrier concentration is extremely important for the functioning of the thermoelectric device, as it determines the position of the equilibrium chemical potential of the electrons with respect to the minibands. In the present case of the InAs/GaAs quantum dots, we assume  $n$ -type conductivity due to electrons supplied by donors predominantly located in the host material. These donors are characterized by a donor concentration  $n_D$  and a charge transfer level  $\varepsilon_D$ . The latter is assumed to lie 10 meV below the bulk conduction band minimum of GaAs for the present example. Moreover, we need to take into account the bulk conduction band states, as these states may be populated by electrons supplied by the donors, and may thus also contribute to the thermoelectric properties. In the following, values from the experimental literature are used for the effective mass of the conduction band electrons of GaAs and InAs. A calculation of the transport relaxation time for carriers in the bulk band yields the well-known increase of  $\tau$  proportional to the square root of the energy measured from the conduction band bottom. While the so-defined model provides us with all the information needed to calculate the electronic part of  $ZT$ , input for the lattice contribution to  $\kappa$  must come from elsewhere. At present, we treat  $\kappa_{\text{ph}}$  as a numerical parameter that can be set to any available experimental value. In the following,  $\kappa_{\text{ph}} = 0.2 \text{ W/(m K)}$  is used.

Results of our model are shown in Fig. 4. We find that the figure of merit  $ZT$  is highly sensitive to the donor concentration  $n_D$  and shows sharp peaks whenever the chemical potential  $\mu$  of the electrons falls into one of the minibands. For a particular geometry, e.g. for  $a_z = 1.566 \text{ nm}$  and  $d_z = 6.26 \text{ nm}$  shown in the left-hand-side panel of Fig. 4, peak values of  $ZT$  in one miniband are as high as  $ZT = 2$ . Further analysis of the factors entering the calculation of  $ZT$  shows that in this miniband regime the thermal conductivity  $\kappa$  is dominated by the lattice contribution  $\kappa_{\text{ph}}$ . While partially occupied minibands contribute already to the electrical conductivity  $\sigma$ , their contribution to  $\kappa_{\text{el}}$  is small because only little entropy can be carried by excitations around the Fermi energy in such a narrow miniband. For high doping concentrations exceeding  $5 \times 10^{25} \text{ m}^{-3}$ , the electron chemical potential rises up to the bulk conduction band. Under these conditions, thermal excitations of the carriers high up into empty states in the conduction band are possible. While  $\sigma$  for the case of bulk transport is higher than for miniband transport only,  $\kappa_{\text{el}}$  increases more steeply than  $\sigma$  with increasing  $n_D$ . Consequently, the figure-of-merit  $ZT$  drops at very high donor concentrations, when the conductivity becomes dominated by the bulk conduction band.

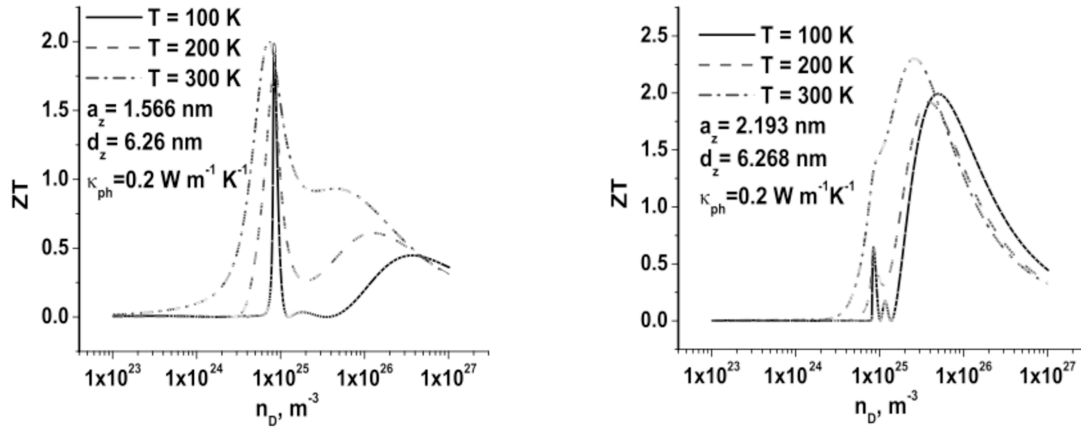


Figure 4. The figure of merit  $ZT$  for a 1D stack of InAs/GaAs QDs with height  $a_z=1.566$  nm and period  $d_z=6.26$  nm (left-hand-side panel) and  $a_z=2.193$  nm and  $d_z=6.268$  nm (right-hand-side panel) calculated as a function of the concentration of donors  $n_D$  with charge transfer level  $\epsilon_D$  at 10 meV below the GaAs conduction band minimum.

Looking at the right-hand-side panel of Fig. 4, one learns that the precise dependence of  $ZT$  on the donor concentration may vary from sample to sample, depending on the geometrical parameters of the InAs quantum dots embedded in the GaAs matrix. In the case of somewhat taller QDs ( $a_z = 2.193$  nm) with a stacking period of  $d_z = 6.268$  nm, the figure of merit both at  $T=200$  K and  $T=300$  K shows a single maximum as function of  $n_D$ . For these geometrical parameters of the QDs, the third miniband in the QD stack comes energetically very close to the onset of the conduction band, and at  $T=300$  K the electrons provided by the donors populate both the highest miniband and the conduction band bottom. Only at low temperatures,  $T=100$  K, small additional peaks at somewhat lower donor concentration  $n_D$  due to the minibands are visible. In contrast to pure bulk GaAs, which has a very low figure of merit at room temperature, we predict a significantly enhanced  $ZT$  due to nanostructuring.  $ZT$  reaches its peak value of 2.3 at  $n_D = 3 \times 10^{25} \text{ m}^{-3}$  at room temperature, due to added contributions from both the minibands and the bulk conduction band, and again drops off for higher donor concentrations, when the conductivity becomes dominated by bulk states.

A more systematic study of the effect of QD geometry on the thermoelectric figure of merit can be found elsewhere [13]. Already from the examples given here, it is clear that QD crystals hold great promise as materials for thermoelectric converters. However, the results also show that a fine-tuning of the geometrical specifications of the QD inclusions and the suitable donor concentration in the samples is required to exploit the potential of these materials. This is an area of research where fabrication and characterization of the nanostructures should be carried out in close collaboration with simulations of their transport properties to obtain samples with optimum performance.

## 5. Summary and Conclusions

Modeling of materials for optimizing their electrical transport properties must start from a quantum-mechanical modeling step, using density functional theory, or, for very large systems, a tight-binding Hamiltonian to describe the electronic structure of the material. For some properties, e.g. band gaps or magnetic moments, employing the cluster expansion technique allows for a direct search for the optimum in a large configuration space. If

dissipative processes play a role for the quantity of interest, as is the case for the thermoelectric figure of merit  $ZT$ , a hierarchical multi-scale approach is recommended. It comprises solving a Boltzmann transport equation with parameters (band dispersion, transport relaxation time) calculated from a microscopic theory.

## Acknowledgements

Financial support from Deutsche Forschungsgemeinschaft within SPP 1386 ‘Nanostructured Thermoelectrics’ and SFB491 ‘Magnetic Heterostructures: Spin structure and spin transport’ is gratefully acknowledged. V.M.F. has been supported by the European Science Foundation through Exchange Grant No. 2157 within the activity ‘Arrays of Quantum Dots and Josephson Junctions’ and by the German Academic Exchange Service (DAAD). We acknowledge fruitful collaboration with O. G. Schmidt and A. Rastelli on quantum dots arrays for thermoelectrics.

## References

- [1] R. A. de Groot, F. M Mueller, P. G. van Engen, and K. H. J. Buschow, *Phys. Rev. Lett.* **50**, 2024 (1983).
- [2] J. M. Sanchez, F. Ducastelle, and D. Gratias, *Physica A* **128**, 334 (1984).
- [3] S. Müller, *J. Phys.: Condens. Matter* **15**, R1429 (2003).
- [4] A. van de Walle and G. Ceder, *J. Phase Equilibria Diffus.* **23**, 348 (2002).
- [5] A. Franceschetti, S. V. Dudiy, S. V. Barabash, A. Zunger, J. Xu, and M. van Schilfgaarde, *Phys. Rev. Lett.* **97**, 047202 (2006).
- [6] A. Franceschetti and A. Zunger, *Nature* **402**, 60 (1999).
- [7] C. D. R. Ludwig, T. Gruhn, C. Felser, T. Schilling, J. Windeln, and P. Kratzer, *Phys. Rev. Lett.* **105**, 025702 (2010).
- [8] B. Hülsen, M. Scheffler and P. Kratzer, *Phys. Rev. B* **78**, 094407 (2009).
- [9] T. Ishikawa, H.-X. Liu, T. Taira, K. Matsuda, T. Uemura, and M. Yamamoto, *Appl. Phys. Lett.* **95**, 232512 (2009).
- [10] B. Hülsen, M. Scheffler and P. Kratzer, *Phys. Rev. Lett.* **103**, 046802 (2009).
- [11] D. Grützmacher, T. Fromherz, C. Dais, J. Stangl, E. Müller, Y. Ekinici, H. H. Solak, H. Sigg, R. T. Lechner, E. Wintersberger, S. Birner, V. Holy, and G. Bauer, *Nano Lett.* **7**, 3150 (2007).
- [12] V. G. Talalaev, G. E. Cirlin, A. A. Tonkikh, N. D. Zakharov, P. Werner, U. Gösele, J. W. Tomm, and T. Elsaesser, *Nanoscale Res. Lett.* **1**, 137 (2006).
- [13] V. M. Fomin and P. Kratzer, *Phys. Rev. B* **82**, in press (2010).
- [14] T. Hammerschmidt, P. Kratzer, and M. Scheffler, *Phys. Rev. B* **77**, 235303 (2008); Erratum: *Phys. Rev. B* **81**, 159905 (2010)
- [15] T. B. Boykin, *Phys. Rev. B* **56**, 9613 (1997)
- [16] R. Santoprete, B. Koiller, R. B. Capaz, P. Kratzer, Q.K.K. Liu, and M. Scheffler, *Phys. Rev. B* **68**, 235311 (2003).
- [17] G. D. Mahan and J.O. Sofo, *Proc. Natl. Acad. Sci. USA* **93**, 7436 (1996).
- [18] T.E. Humphrey and H. Linke, *Phys. Rev. Lett.* **94**, 096601 (2005).
- [19] G. Pernot, M. Stoffel, I. Savic, F. Pezzoli, P. Chen, G. Savelli, A. Jacquot, J. Schumann, U. Denker, I. Mönch, Ch. Deneke, O. G. Schmidt, J. M. Rampnoux, S. Wang, M. Plissonnier, A. Rastelli, S. Dilhaire, and N. Mingo, *Nature Materials* **9**, 491 (2010).
- [20] A. A. Balandin and O. L. Lazarenkova, *Appl. Phys. Lett.* **82**, 415 (2003).

## Micromechanical modeling of ferroelectric bulk materials in the context of a multiscale simulation chain

Lothar Kunz<sup>1,2</sup>, Alexander Konstandin<sup>1</sup>, Monika Gall<sup>3</sup>, Eberhard Hennig<sup>4</sup>, Hans-Jürgen Schreiner<sup>5</sup> and Marc Kamlah<sup>2</sup>

<sup>1</sup> Corporate Sector Research and Advance Engineering, Robert Bosch GmbH,  
70049 Stuttgart, Germany

<sup>2</sup> IMF II, Karlsruhe Institut of Technology, 76344 Eggenstein-Leopoldshafen, Germany

<sup>3</sup> Fraunhofer-Institut für Werkstoffmechanik IWM, 79108 Freiburg, Germany

<sup>4</sup> PI Ceramic GmbH, 07589 Lederhose, Germany

<sup>5</sup> Geschäftsbereich Multifunktionskeramik, CeramTec AG, 91207 Lauf, Germany

[alexander.konstandin@de.bosch.com](mailto:alexander.konstandin@de.bosch.com)

In a multiscale simulation approach for ferroelectric materials, micromechanical modeling of grain structures yields the behavior under electrical and mechanical loading at small or large signal loading, as used for characterising the material experimentally on a macroscopic level.

As part of this chain a micromechanical model based on the constitutive law by Huber et al. [1, 2] is developed and implemented in the finite element software FEAP. The parameters of the constitutive law are calibrated against data obtained from the phase field approach of B. Völker et al. For this purpose, phase field simulation results were homogenized in order to retrieve material tensors for the description of the piezoelectric behaviour (small signal) on the microscopic scale. Further, the domain evolution of the phase field models was used to calibrate the switching behaviour of the Huber-Fleck model for ferroelectric simulations (large signal).

We present results on the dependence of piezoelectric and ferroelectric behaviour averaged over polycrystals on the grain size and shape. The outcome is also compared with experimental data obtained from Al and Nb doped PZT compositions investigated in this project. The results proof the general possibility of multiscale simulations for ferroelectrics, but also identify computational and theoretical deficiencies on each scale.

[1] J. E. Huber et al., J. Mech. Phys. Sol. **47** (1999) 1663-1697

[2] A. Pathak, R. M. McMeeking, J. Mech. Phys. Sol. **56** (2008) 663-683

Acknowledgement: This work was funded by the German Federal Ministry of Education and Research (BMBF Framework Programme WING, Project Code 03X0510).

# Ab-initio study of Cu and Fe doping in the lead-free ferroelectric perovskite potassium sodium niobate

**Sabine Körbel<sup>1</sup>, Pavel Marton<sup>1</sup>, and Christian Elsässer<sup>1,2</sup>**

<sup>1</sup>Fraunhofer Institute for Mechanics of Materials IWM, Wöhlerstraße 11, 79108 Freiburg, Germany

<sup>2</sup>IZBS, Karlsruhe Institute of Technology, Kaiserstr. 12, 76131 Karlsruhe, Germany  
sabine.koerbel@iwm.fraunhofer.de

Potassium sodium niobate ( $K_xNa_{1-x}NbO_3$ , KNN) is regarded as a possible nontoxic future substitute for lead zirconate titanate ( $PbZr_xTi_{1-x}O_3$ , PZT), which is currently the material of choice for many piezoelectric applications.

Point defects in these materials are generated as well accidentally as on purpose, since the ferroelectric properties are commonly tailored by doping with aliovalent metals. In addition it was found that adding CuO positively influences the sintering behaviour of ceramic KNN.

Hard or soft ferroelectric behaviour is commonly attributed to point defects. In the case of hard ferroelectrics, it is assumed that defect dipoles consisting of acceptor dopants on the *B* site in the perovskite structure  $ABO_3$ , associated with oxygen vacancies for charge compensation, pin the polarisation and therefore impede domain wall motions. Theoretical ab-initio studies of Cu and Fe doping in  $PbTiO_3$  have revealed that the defect dipoles tend to align with the direction of the ferroelectric polarisation [1]. An experimental study on  $BaTiO_3$  and  $PbTiO_3$  has shown that the reversed effect is also possible, i.e. the defect dipoles can act as a restoring force for the polarisation, which enables reversible switching by  $90^\circ$ , accompanied by a large strain [2].

In this work, ab-initio calculations, by means of density functional theory (DFT) in the local density approximation, are employed to investigate KNN doped with Cu and Fe as substitutional aliovalent elements. We present an analysis of the preferred lattice sites for the two dopants as function of the processing conditions, namely the oxygen partial pressure, and of the alkali-metal stoichiometry, and we compare the energetic stability of several conceivable defect complexes of Cu dopants and vacancies in KNN [3].

We demonstrate how isolated substitutional  $Cu_{Nb}$  atoms deform the ferroelectric energy hypersurface, on which the polarisation switching takes place, along certain transition paths connecting different ferroelectric phases in  $KNbO_3$ .

Preliminary results of atomistic simulations for the reorientation of the polarisation will also be presented.

[1] P. Erhart et al, Phys. Rev. B **76** (2007), 174116.

[2] X. Ren, Nature Materials **3** (2004), 91.

[3] E. Erünal et al, Functional Materials Letters **3** (2010).

Acknowledgement: This work is supported by the German Research Foundation (DFG, project EL 155/21-1).

# Tight Binding Models from LCAO

**Georg K. H. Madsen, Eunan J. McEniry and Ralf Drautz**

ICAMS, Ruhr-Universität Bochum, Stiepelers Strasse 129, 44801 Bochum, Germany  
georg.madsen@rub.de

Tight Binding (TB) methods can be seen as a parameterization of Linear Combination of Atomic Orbitals (LCAO) -methods, where the matrix elements of the Hamiltonian are parametrized and the rest of the DFT energy is approximated by terms dependent only on the atomic positions. In their modern formulation TB methods can treat charge transfer and spin-polarisation, making them a robust compromise of accuracy and transferability versus computational cost and an attractive intermediate between DFT and empirical interatomic potentials.

We will present a methodology for down-folding the LCAO Hamiltonian to a short ranged minimal basis. This has a practical advantage in making the construction of the TB model simpler and offers a more direct link between the TB and DFT energy functionals, thus facilitating future method development. We will highlight the differences between a flexible LCAO basis and the one used in an efficient TB-model. The methodology will be applied to calculate the trend in the TB basis when moving across the 3d series and it will be shown how it can be parameterized as two-center bond integrals.

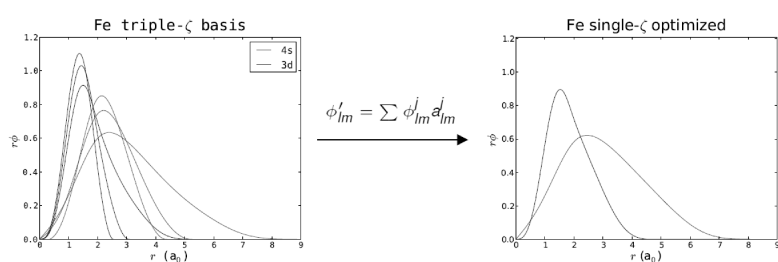


Figure: Radial part of s and d pseudo basis functions of Iron. Left) The full triple- $\zeta$  basis used for DFT. Right) The down-folded minimal basis used for TB parameterization.

Finally the modeling of light elements from the second period will be discussed.

# Comparison of the Deformation Behavior of Digital Materials using Full-field Strain Analysis and Micromechanical Modeling

**Franz Hiptmair<sup>1</sup>, Martin Reiter<sup>1</sup> and Zoltan Major<sup>1</sup>,**

**<sup>1</sup>Institute of Polymer Product Engineering,  
Johannes Kepler University Linz  
Altenbergerstrasse 69, 4040 Linz, Austria**

## ABSTRACT

Existing digital materials over a wide modulus range were provided by the company for this study and included two types of compounds: an elastomer like matrix, filled with hard particles (Type 1) and a hard matrix, filled with elastomer particles (Type 2). The material data as input for the micromechanical simulation and the properties of the compounds for comparing to the results of the simulation were determined in tensile tests applying an additional full-field strain analysis device [1]. In the micromechanical simulations the homogenization technique of the Digimat MF Software module as well as finite element tools (Digimat FE & Abaqus) were applied. The simulations were first carried out in the elastic deformation regime under tensile conditions and the calculated Young's modulus and Poisson's ratio values were compared with the experimental data determined by full-field strain analysis. Furthermore, special emphasis was devoted to extend the simulations towards large strains by applying proper hyperelastic models and functions.

## 1. Introduction

Recently, a novel PolyJet prototyping device (Objet Geometries Ltd, Israel) for 3D multi-material printing was introduced. In addition to the conventional application of this device, the rapid prototyping of various components and products in the design phase, a novel application is targeted. Due to the special capabilities of this machine, novel material compounds termed as "digital materials" can be produced. The company provides materials over a wide elastic modulus range from approx. 1 MPa up to 3500 MPa. While the low modulus materials (1 to 5 MPa) correspond to the mechanical behavior of elastomers, the high modulus materials can be used to simulate the deformation behavior of thermoplastic polymers.

Two types of digital materials were produced and provided by Objet for this study as tensile specimens: (a) Type1, flexible compound, soft matrix (TangoBlackPlus) +various amount of hard inclusions (VeroWhite) and (b) Type 2, rigid compound, hard matrix (VeroWhite) + various amount of soft inclusions (TangoBlackPlus).

The digital compounding provides novel perspectives for a rapid material development. However, one should take care when interpreting the results and the simulation must always be verified by proper experiments.

## 2. Experimental Data

To acquire the input data for the simulation, the Digital materials as well as the neat primary materials were measured in tensile tests. Modulus and Poisson's ratio values were determined via an optical strain analysis device (ARAMIS, GOM, Braunschweig, D).

The Shore hardness dependence of Young's modulus and Poisson's ratio values for the type 1 digital materials is represented in Figure 1. It was found that the Poisson's ratio gives a linear correlation with the Shore hardness up to  $HS_A$  85, whereas with increasing Shore hardness a nonlinear increase of the Young's modulus was observed.

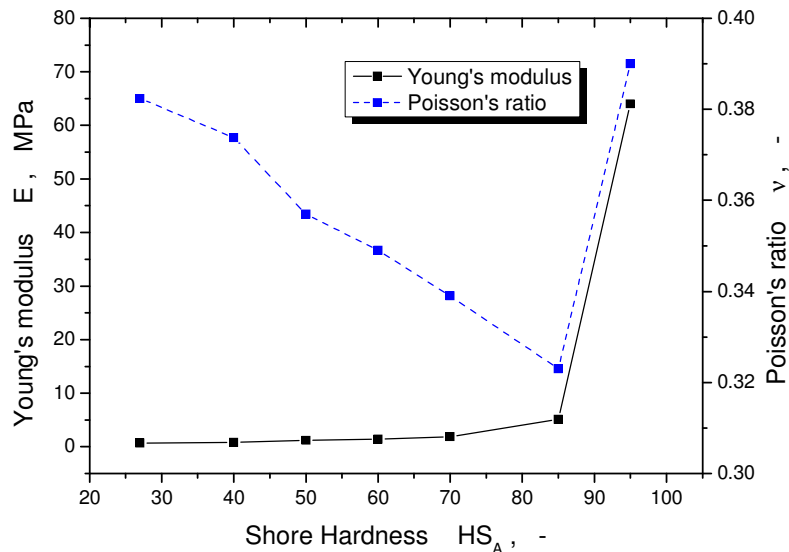


Fig.1: Young's modulus and Poisson's ratios versus Shore hardness for Type 1 digital materials

## 3. Micromechanics Simulations in the Elastic Deformation Regime

To model the tensile loading for any Digital compound a series of Digimat-MF simulations has been carried out over the whole range of volume fractions. As a first approximation an elastic material model was applied for both phases. The input parameters were experimentally determined as stated above and are given in Table 1. The inclusion shape was assumed to be spherical. For the Mean-field homogenization the Double-Inclusion model has turned out to be most applicable [2].

Table 1: Parameters used in the mechanical analysis

TangoBlackPlus	Young's modulus	0.67
	Poisson's ratio	0.38238
VeroWhite	Young's modulus	380
	Poisson's ratio	0.459

The constituent volume fraction dependence of Young's modulus values are shown in Fig. 2 for both Type 1 and Type 2 compounds. The straight line represents the soft matrix-hard inclusion (Type 1) compound, the dot line corresponds to the hard matrix soft particle (Type 2) compound. The results clearly indicate the limitation of a simple homogenization procedure by using the Double Inclusion approach. Beyond a particle content of 20 % a significant difference is observed between the two simulation routes.

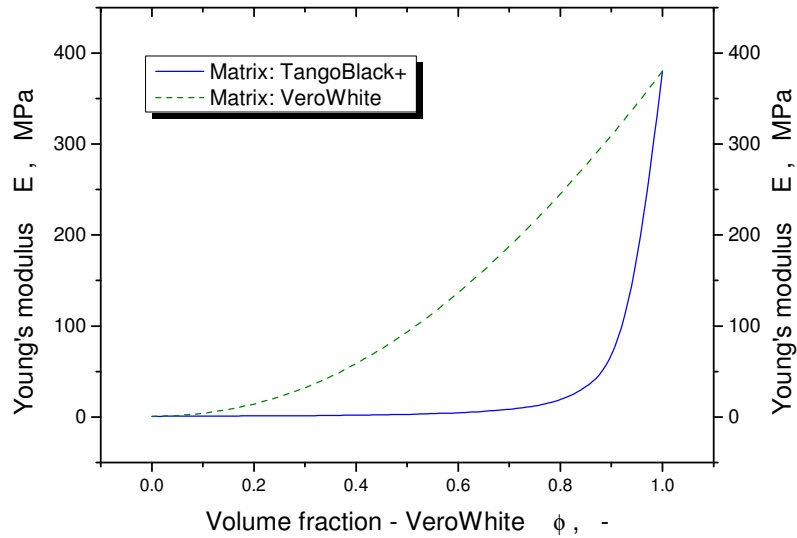


Fig.2: Constituent's volume fraction dependence of Young's modulus values

The deviation between both curves reveals that the digital materials mechanical properties are highly dependant on which one forms the matrix and which one forms the inclusions.

In order to improve simulation quality, in addition to the homogenization approach the finite element method (Digimat FE & Abaqus) was also applied and the mechanical properties were calculated. For this, several  $\mu$ -cells with volume fractions ranging from five to 37.5 % were generated in Digimat FE while the actual loading steps were performed in Abaqus using periodic boundary conditions. The mechanical input parameters were again taken from Tab 1.

The comparison of Poisson's ratio values (simulated by homogenization and by FE) with experimental data is shown in Fig. 3. The Poisson's ratio was calculated from the volumetric mean values of the lateral strains in the  $\mu$ -cell. The volume fractions for the digital materials have been determined by correlation of the experimental tensile modulus data (Fig. 1) with the MF and FE results.

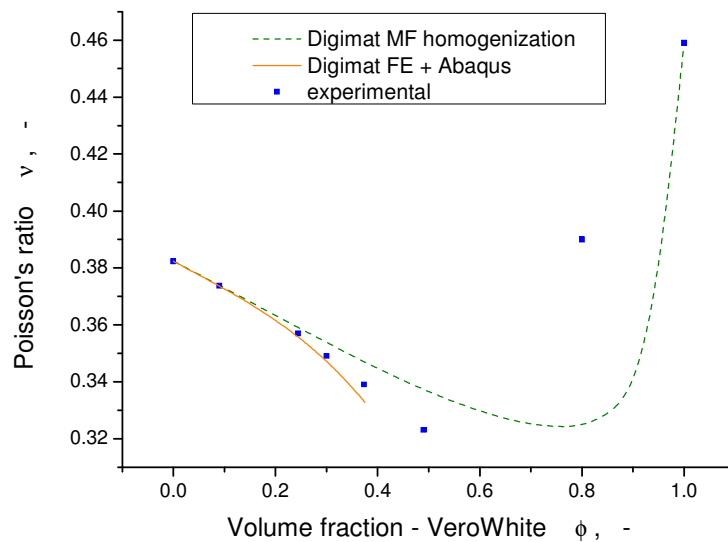


Fig.3: Comparison of the Poisson's ratios calculated with Digimat MF, obtained by FEA and experimentally determined values for a Type 1 digital material

Above 25 % there is an increasing deviation between homogenization and experiment and as expected the FE provides better agreement.

#### 4. Micromechanics Simulations using Hyperelastic Models

To extend the simulations towards large strains, in addition to the simple elastic models, hyperelastic models were applied. The respective parameters were determined via the Abaqus material data evaluation feature [3]. Since VeroWhite revealed significantly higher stiffness and therefore only would undergo very minor deformations, an ideally elastic behaviour could be assumed for the Inclusion phase. The simulated nominal stress-strain curves (Ogden Hyperelastic model with two pairs) for Tango Black Plus and for the digital materials are shown and compared with the experimental curves in Fig. 4. In spite of the fact that the accurate material morphology is not known, a good agreement was found between the simulation and the experiments.

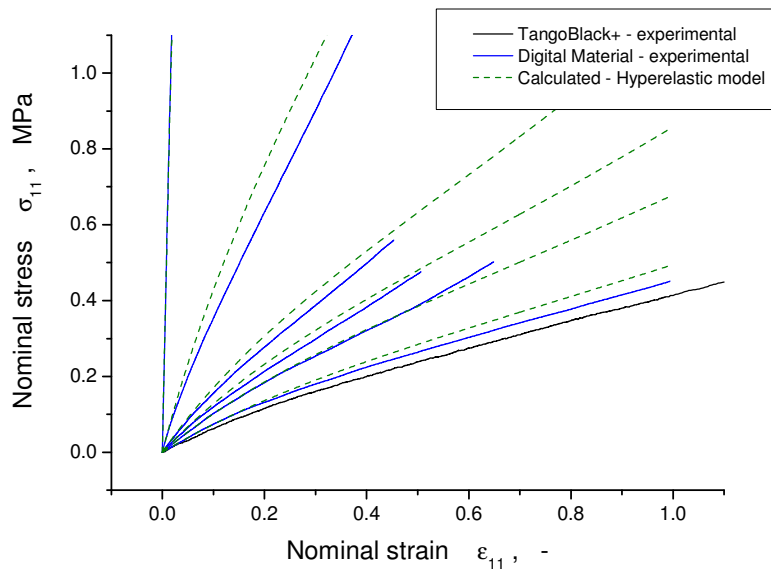


Fig.4: Experimental and simulated nominal stress-strain curves for Tango Black Plus and for Type 1 digital materials

The deviations for larger strains can be partly explained by the fact that strictly speaking the Ogden model is applicable for incompressible materials only. Moreover for all the materials involved in this study the tensile response was found to be a function of the strain rate, whereas hyperelastic models do not account for such rate dependent behaviour.

Finally, these digital materials can be used for calibrating material models in micromechanics simulations. For this purpose however, detailed knowledge of the morphology is necessary. Hence, future work will focus on the microstructure characterization of the digital materials and the refinement of the hyperelastic models used for micromechanics simulations of soft polymeric materials.

#### References

- [1] Jerabek M., Major Z., Lang R.W.: *Strain determination of polymeric materials using digital image correlation*; Polymer Testing, **29**, 407-416 (2010)
- [2] Digimat 4.0.2 Manual; e-Xstream engineering (2010)
- [3] Abaqus 6.9.2 Manual; Dassault Systèmes (2009)

# Development and application of tight-binding potentials for Ti-C and Ti-N systems

**E. R. Margine<sup>1</sup>, M. Reese<sup>2,3</sup>, M. Mrovec<sup>2,3</sup>, C. Elsässer<sup>2,3</sup>, A. N. Kolmogorov<sup>4</sup>  
R. Drautz<sup>5</sup> and D. Pettifor<sup>4</sup>**

<sup>1</sup>Department of Materials, University of Oxford, Oxford Parks Road, OX1 3PH, UK  
(roxana.margine@materials.ox.ac.uk)

<sup>2</sup>Fraunhofer-Institute for Mechanics of Materials IWM, Wöhlerstraße 11,  
79108 Freiburg, Germany

<sup>3</sup>IZBS, Karlsruhe Institute of Technology,  
Kaiserstraße 12, 76131 Karlsruhe, Germany

<sup>4</sup>Department of Materials, University of Oxford, Oxford Parks Road, OX1 3PH, UK

<sup>5</sup>Department of Atomistic Modelling and Simulation, ICAMS, Ruhr-Universität Bochum,  
Stiepelers Straße 129, 44801 Bochum, Germany

Titanium carbides and nitrides are among the hardest materials used for nanocomposite coating applications. Atomistic simulations can be performed to further tune the materials' mechanical properties if a robust model can be found to provide an accurate and efficient description of complex interfaces with thousands of atoms. We develop an orthogonal p-d tight binding (TB) model with an explicit treatment of the charge transfer and explore its transferability to environments relevant in the Ti-C and Ti-N systems. The parameterization is done using a dataset of band structures, binding energies, defect energies, and elastic constants calculated within the density functional theory. This TB model is applied to comparing and contrasting the behaviour of TiC and TiN surfaces.

# First-principles study of ferroelectric lead zirconate titanate for development of a multi-scale simulation chain

**Pavel Marton<sup>1</sup>, Sabine Körbel<sup>1</sup>, and Christian Elsässer<sup>1,2</sup>**

<sup>1</sup>Fraunhofer Institute for Mechanics of Materials IWM, Wöhlerstraße 11, 79108 Freiburg, Germany

<sup>2</sup>IZBS, Karlsruhe Institute of Technology, Kaiserstr. 12, 76131 Karlsruhe, Germany  
[pavel.marton@iw.fraunhofer.de](mailto:pavel.marton@iw.fraunhofer.de)

Lead zirconate titanate (PZT) and lead titanate (PTO) are piezoelectric ceramic materials used in a variety of applications like actuators, sensors, or resonators. Their complicated microstructure and the sensitivity of the ferroelectric state to the experimental conditions render the local observation of intrinsic properties and nano-sized structures, like domain walls (DW) and grain boundaries (GB), challenging and rare.

Therefore, a multi-scale hierarchical approach was set up in the project “Computational Modelling of Ferroelectric Materials” (COMFEM) to obtain macroscopic properties of PZT from first principles, by means of density functional theory (DFT), atomistic shell-model simulation, phase-field theory, and micromechanical modelling. Particular attention was paid to the transfer of material parameters between individual levels.

An objective of this part of COMFEM was to provide data for the development of a phase-field model for PZT. To this end, we employed first-principles calculations and shell-model simulations to study intrinsic properties of PZT, namely atomic structure, spontaneous polarization, elastic and piezoelectric tensors, for various ordered arrangements of Zr and Ti atoms, and for statistically homogeneous disorder of Zr and Ti. We also determined the energy and the thickness of 180° and 90° DWs in the tetragonal phase. An estimation of the coercive electric field for switching the spontaneous polarization by shifting a DW suggested that a “nucleation and growth” mechanism governs the motion of both types of DWs, in contrast to the usually assumed plane-like DW displacement mechanism. Finally, we consider a ferroelectrically “hard” point-defect complex of an iron atom and an oxygen vacancy in the ferroelectric PTO. Barriers for switching of such a defect complex by oxygen migration are presented and interpreted.

This work was funded by the German Federal Ministry of Education and Research (BMBF Programme WING, Project Code 03X0510).

# Multiscale Modeling of Structure and Electronic Transport in Multifunctional Materials

Robert Maul, Ivan Kondov, and Wolfgang Wenzel

Karlsruhe Institute of Technology,  
Institute of Nanotechnology and Steinbuch Centre for Computing  
PO Box 3640, D-76021 Karlsruhe, Germany

The study of the correlation between structure and electron transport properties at the molecular or even atomic scale has generated many striking insights in the last decade. Promising new functional materials and nanoscale devices developed recently employ physical effects at the quantum mechanics scale for novel molecular functionality. Therefore, a reasonable multiscale model of such materials have to take the quantum transport level into account.

In recent years we have therefore pursued simulation methods, which connect continuum models and atomistic models down to quantum mechanics scale, leading to new insights into the functionality of novel active nano-devices. Here we present simulations of charge transport in ordered and disordered trishydroxyquinoline-aluminum used for organic light emitting diodes. Our calculations are the first of their kind to explicitly consider individual molecules and their amorphous packing in three dimensions. Using this approach, we are able to reproduce experimental mobilities without the need for any fitting parameters. In addition we apply our multiscale model to explain the operation of an atomic-scale three-terminal device by a novel switching mechanism of bistable, self-stabilizing reconstruction of the electrode contacts at the atomic level.

F. Q. Xie, R. Maul, S. Brendelberger, C. Obermair, E. B. Starikov, W. Wenzel, G. Schön, and T. Schimmel, *Applied Physics Letters* **93** (4), 3 (2008)

F. Q. Xie, R. Maul, A. Augenstein, C. Obermair, E. B. Starikov, G. Schön, T. Schimmel, and W. Wenzel, *Nano Letters* **8** (12), 4493 (2008)

S. Behrens, A. Heyman, R. Maul, S. Essig, S. Steigerwald, A. Quintilla, W. Wenzel, J. Bürck, O. Dgany, O. Shoseyov, *Advanced Materials* **21**, 3437 (2009)

F. Q. Xie, R. Maul, Ch. Obermair, W. Wenzel, G. Schön, Th. Schimmel, *Advanced Materials* **22**, 2036 (2010)

## **Tight-binding modelling of iron and steel**

**Eunan J. McEniry, Georg K. H. Madsen and Ralf Drautz**

ICAMS, Ruhr-Universität Bochum, Stiepel Strasse 129, 44801 Bochum, Germany.  
eunan.mceniry@rub.de

In order to perform atomistic simulations of steels, it is necessary to have a detailed understanding of the complex interatomic interactions in the material. The tight-binding approximation provides an computationally efficient, yet accurate, method to investigate such interactions.

In the present work, a tight-binding model for iron, including magnetism, has been parameterised from ab-initio density-functional calculations, and its transferability between various structures is discussed.

To describe the effects of alloying in steel, it is necessary to consider other transition metals, and light elements, which have a significant effect on the mechanical properties of the steel. We show how this is achieved within the present methodology.

We will demonstrate, by numerical simulation, the application of the method to various structures, and compare the results to full ab-initio calculations.

## From DFT to Tight-Binding by Utilizing an Optimized Minimal Basis

**Bernd Meyer<sup>1</sup>, Alexander Urban<sup>1</sup>, Martin Reese<sup>2</sup>, Matous Mrovec<sup>2</sup>,  
and Christian Elsässer<sup>2</sup>**

<sup>1</sup>Interdisciplinary Center for Molecular Materials ICMM and  
Computer-Chemistry-Center CCC, University Erlangen-Nürnberg, Germany

<sup>2</sup>Fraunhofer Institute for Mechanics of Materials IWM, Freiburg, Germany

bernd.meyer@chemie.uni-erlangen.de

The most common approach to derive tight-binding models for practical calculations is to fit band structures and total energies to the results of DFT calculations or experimental data. In this talk an alternative approach will be presented which significantly reduces the amount of required fitting. The method is based on a projection of fully converged (with respect to basis set size) wave functions from plane-wave-based DFT computations onto a minimal basis of atomic orbitals. The radial shape of the atomic orbital basis functions is optimized by minimizing the loss (spillage) in the projection procedure. Subsequently, the Slater-Koster tables are calculated with the optimized minimal basis using the fully converged DFT Hamiltonian. To demonstrate the high quality of the derived TB parameterizations results for the electronic structure for different benchmark calculations will be compared to DFT reference data.

## Bond-order potentials for transition metals and their compounds

**Matous Mrovec<sup>1,2,\*</sup>, Martin Reese<sup>2,1</sup> and Christian Elsässer<sup>1,2</sup>**

<sup>1</sup>Fraunhofer IWM, Wöhlerstr. 11, 79108 Freiburg, Germany

<sup>2</sup>IZBS, Karlsruhe Institute of Technology, Kaiserstr. 12, 76131 Karlsruhe, Germany

\* matous.mrovec@iwm.fraunhofer.de

Bond-order potentials (BOPs) provide a real-space semi-empirical description of interactions between atoms based on the chemically intuitive tight-binding approximation for the electronic structure. The BOP approach offers two key advantages that are crucial for a successful modeling of extended crystal defects in covalent materials and transition metals. First, due to its quantum mechanical character it conveys a physically sound description of chemical bonding rather than ad hoc functional forms, which are common to classical empirical interatomic potentials. Second, its real space parameterization and computational efficiency enables to carry out computer simulations of large and complex systems, which are usually inaccessible to rigorous first-principles electronic-structure methods. We will review the theoretical background of the atom-based bond-order potential formalism and discuss latest developments for transition metals and their compounds. The applicability of BOPs will be demonstrated on studies of extended defects, in particular dislocations and grain boundaries. An assessment of the transferability of BOPs and comparison to both higher-level electronic-structure methods and to empirical many-body potentials will be presented.

## **Interaction of H with vacancies in iron and steels: The combination of atomistic, thermodynamic and elastic effects**

**Roman Nazarov<sup>1</sup>, Tilmann Hicel<sup>1</sup> and Jörg Neugebauer<sup>1</sup>**

<sup>1</sup>Max-Planck-Institut für Eisenforschung GmbH, Computational Materials Design, Max-Planck-Straße 1, D-40237 Düsseldorf, Germany  
r.nazarov@mpie.de

Several embrittlement mechanisms are associated with a significant increase of the vacancy concentration in an H-rich atmosphere. Due to the interaction of the vacancies with the hydrogen contained in the material, a formation of brittle phases or voids can be initiated, which interact with dislocations and microcracks. The resulting fracture is an important problem for the design of new structural materials such as modern high-strength steels.

In order to reveal the physics of such phenomena, we have coupled state-of-the-art ab initio techniques with classical thermodynamics and kinetic Monte-Carlo simulations. Our systematic comparison of isolated and hydrogen loaded vacancies in fcc iron with various magnetic configurations reveals that hydrogen reduces the formation energy of a vacancy. This decrease can be significant, as up to 6 hydrogen atoms can be incorporated into a vacancy.

Based on our ab-initio results we developed a thermodynamic model which determines the concentrations of vacancies, of hydrogen in different interstitial positions and of vacancy-hydrogen complexes as a function of pressure, temperature and external hydrogen chemical potential. Applying this model we find dramatically increased vacancy concentrations and total hydrogen concentrations in fcc iron if the material is exposed to a H-rich atmosphere. Our predicted vacancy concentrations are in excellent agreement with available experimental data.

# **Engineering Domain Switching Dynamics in Ferroelectrics via Electric Field Control – Investigation using 3D Phase Field Modeling**

**Nathaniel Ng, Rajeev Ahluwalia and David J. Srolovitz**

Institute of High Performance Computing, 1 Fusionopolis Way #16-16 Connexis,  
Singapore 138632  
ngkc@ihpc.a-star.edu.sg

Domain switching dynamics are very strongly controlled by the patterning of the electrodes in ferroelectric thin film. Electrodes can be patterned so that the electric field is approximately parallel to the surface as in the case of interdigitated electrodes, perpendicular to the film surface, as in a ferroelectric capacitor, and more complex arrangements can result in very different switching dynamics. It has already been shown that fringing electric fields due to an electrode edge or from patterning the surface morphology [Ahluwalia et al., *Nanotechnology*, 20(44), 445709 (2009)] result in electric field vectors diagonal to the film surface possibly resulting in different nucleation pathways during switching. In more complex arrangements, the top electrode could be offset relative to the bottom electrode, or fringing electric fields in the vicinity of a piezoforce microscopy (PFM) tip. To study these effects, we employ the time-dependent Ginzburg-Landau (TDGL) model using a real space method as described in our earlier work [Ng et al., *Acta Materialia*, 57(7), 2047 (2009)], which has recently been developed into a full 3D framework with full electrostatic and elastic effects. The advantage of this framework is that equations are solved entirely in real space using finite differences allowing ease of applying the boundary conditions. Boundary conditions vary from completely uncompensated charge at the free surfaces, to fully compensated charge at the electrodes. Simulation results show equilibrium domain structures with polarization vectors parallel to the film at the free surfaces, as well as the effects of fringing electric fields on domain patterns.

# Thermodynamics Modelling of Plasticity: Relating Macroscopic Behaviour to Atomistics via Crystal Defects Control

**P. E. J. Rivera-Diaz-del-Castillo<sup>1</sup>**

<sup>1</sup>Department of Materials Science and Metallurgy, University of Cambridge, Pembroke Street, CB2 3QZ Cambridge, United Kingdom; [pejr2@cam.ac.uk](mailto:pejr2@cam.ac.uk)

A new approach to model plasticity employing irreversible thermodynamics concepts is reviewed. The theory incorporates the contributions of dislocation formation, annihilation and glide into describing the deformation of single crystals and coarse-grained polycrystals, ultra-fine grained and nanocrystalline alloys. The description is based on determining the overall dislocation density of the system. It is shown that the key parameter for describing the hardening behaviour, and to increase the ductility of such systems is the activation energy for dislocation annihilation ( $Q_D$ ), which can be obtained directly from atomistic calculations. The theory is then applied to the description of hot deformation in industrial alloys, highlighting the role played by composition in modifying  $Q_D$ , and showing how it is possible to describe the stress-strain curve of single-phase ferrous systems for various temperatures, strain rates and compositional scenarios. Our recent attempts to describe non-homogeneous distributions of dislocation densities are discussed. The ability for dislocations to cluster in the form of cells and subgrains, and to form patterns such as twins, martensite and deformation bands is tackled. Landau polynomials are employed to describe such dislocations patterns; it is discussed how the coefficients of such polynomials may be computed using various atomistic approaches. The polynomials may be input into the Ginzburg-Landau equation for non-conservative fields for describing the kinetics of dislocation patterning. It is discussed how to quantify the kinetic response of a material to the formation of martensite, stacking faults and/or twins employing first principles calculations.

# On the Multiscale Modeling of Electro-Mechanically Coupled Materials

Jörg Schröder, Marc-André Keip

Universität Duisburg-Essen, Fakultät für Ingenieurwissenschaften,  
Abteilung Bauwissenschaften, Institut für Mechanik, Universitätsstr. 15, D-45117 Essen,  
j.schroeder@uni-due.de, marc-andre.keip@uni-due.de

## ABSTRACT

In this contribution, a meso-macro transition procedure for electro-mechanically coupled materials is presented. The utilized mesoscopic material model is introduced and implemented into an  $FE^2$ -homogenization approach. The resulting two-scale formulation is capable of computing macroscopic boundary value problems under consideration of attached heterogeneous representative volume elements at each macroscopic point. The presented direct homogenization procedure also allows for the efficient computation of effective elastic, piezoelectric, and dielectric coefficients of heterogeneous materials.

## 1. Introduction

The effective properties of a material play an essential role for the macroscopic modeling of micro-heterogeneous and polycrystalline materials. In this regard, the derivation of upper and lower bounds and the computation of estimates for the overall properties have to be distinguished. The estimates of such bounds are based on the fundamental works [1] and later [2–4], and more recently [5]. These methods have been applied for the prediction of mechanical as well as non-mechanical properties. In [6] exact results for the overall properties of piezoelectric composites have been established. Utilizing a unit-cell method, [7] investigated the relation between effective properties and different geometries of microvoids based on a 3-D finite element analysis. An algorithm for the description of micro-heterogeneous coupled thermo-electromagnetic continua has been presented in [8]. In the following a general direct homogenization procedure is presented which couples the macroscopic to the mesoscopic scale, see also [9–17].

The procedure is as follows:

1. Localize suitable macroscopic quantities (e.g. strains and electric field) at each macroscopic point to the mesoscale. To be more specific, apply constraint or boundary conditions on a representative volume element, see e.g. [18] and [19].
2. Solve the mechanical and electrical balance equations on the mesoscale under the applied macroscopic loading in order to obtain the dual mesoscopic quantities (e.g. the stresses and the electric displacements).
3. Perform a homogenization step, i.e. compute the average values of the dual mesoscopic quantities. Transfer these macroscopic variables to the associated points of the macroscale.
4. Solve the electro-mechanically coupled boundary value problem on the macroscale and proceed with step 1 until convergence is obtained on both scales. The numerical solution is based on separate finite element analyses on each scale. The overall algorithmic moduli needed for the Newton-Raphson iteration scheme on the macroscale are efficiently computed during the standard solution procedure on the mesoscale.

## 2. Boundary Value Problems on the Macro- and the Mesoscale

In the following the electro-mechanically coupled boundary value problems (BVP) on both scales are described. The material behavior for the individual constituents on the mesoscale are modeled within a coordinate invariant formulation. Here we restrict ourselves to transversely isotropic material behavior as presented in [20–22], see also Section 4.

### 2.1 Macroscopic Electro-Mechanically Coupled Boundary Value Problem

The body of interest  $\mathcal{B} \subset \mathbb{R}^3$  on the macroscopic scale is parameterized in  $\bar{\mathbf{x}}$ .  $\bar{\mathbf{u}}$  and  $\bar{\phi}$  denote the macroscopic displacement field and the macroscopic electric potential, respectively. The basic kinematic and electric variables are the linear strain tensor and the electric field vector

$$\bar{\boldsymbol{\varepsilon}}(\bar{\mathbf{x}}) := \text{sym}[\bar{\nabla}\bar{\mathbf{u}}(\bar{\mathbf{x}})] \quad \text{and} \quad \bar{\mathbf{E}}(\bar{\mathbf{x}}) := -\bar{\nabla}\bar{\phi}(\bar{\mathbf{x}}) \quad (1)$$

where  $\bar{\nabla}$  denotes the gradient operator w.r.t.  $\bar{\mathbf{x}}$ . The governing field equations for the quasi-static case are the balance of linear momentum and Gauß's law

$$\text{div}_{\bar{\mathbf{x}}}[\bar{\boldsymbol{\sigma}}] + \bar{\mathbf{f}} = \mathbf{0} \quad \text{and} \quad \text{div}_{\bar{\mathbf{x}}}[\bar{\mathbf{D}}] = \bar{q} \quad \forall \bar{\mathbf{x}} \in \mathcal{B}, \quad (2)$$

where  $\text{div}_{\bar{\mathbf{x}}}$  denotes the divergence operator with respect to  $\bar{\mathbf{x}}$ ,  $\bar{\boldsymbol{\sigma}}$  represents the symmetric Cauchy stress tensor,  $\bar{\mathbf{f}}$  is the given body force,  $\bar{\mathbf{D}}$  denotes the vector of electric displacements and  $\bar{q}$  is the given density of free charge carriers. To treat the electromechanical BVP, the surface of the considered body is decomposed into mechanical parts, i.e.  $\partial\mathcal{B}_u \cup \partial\mathcal{B}_\sigma = \partial\mathcal{B}$  with  $\partial\mathcal{B}_u \cap \partial\mathcal{B}_\sigma = \emptyset$  and electrical parts, i.e.  $\partial\mathcal{B}_\phi \cup \partial\mathcal{B}_D = \partial\mathcal{B}$  with  $\partial\mathcal{B}_\phi \cap \partial\mathcal{B}_D = \emptyset$ . The boundary conditions for the displacements and the surface tractions  $\bar{\mathbf{t}}$  are  $\bar{\mathbf{u}} = \bar{\mathbf{u}}_b$  on  $\partial\mathcal{B}_u$  and  $\bar{\mathbf{t}} = \bar{\boldsymbol{\sigma}} \cdot \bar{\mathbf{n}}$  on  $\partial\mathcal{B}_\sigma$ . The boundary conditions for the electric potential and the electric surface charge  $\bar{Q}$  are  $\bar{\phi} = \bar{\phi}_b$  on  $\partial\mathcal{B}_\phi$  and  $-\bar{Q} = \bar{\mathbf{D}} \cdot \bar{\mathbf{n}}$  on  $\partial\mathcal{B}_D$ , where  $\bar{\mathbf{n}}$  is a unit vector perpendicular to the surface and directed outwards from the volume, see Fig. 1.

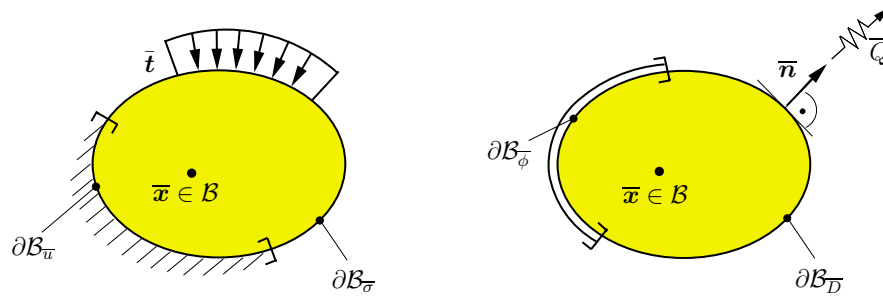


Figure 1: Boundary decomposition of  $\partial\mathcal{B}$  into mechanical and electrical parts and corresponding boundary conditions.

Instead of postulating the existence of a thermodynamical potential on the macroscale, we attach a representative volume element ( $\mathcal{RVE}$ ) at each macroscopic point  $\bar{\mathbf{x}}$ , see Fig. 2.

In order to link the macroscopic variables  $\{\bar{\boldsymbol{\varepsilon}}, \bar{\boldsymbol{\sigma}}, \bar{\mathbf{E}}, \bar{\mathbf{D}}\}$  with their microscopic counterparts  $\{\boldsymbol{\varepsilon}, \boldsymbol{\sigma}, \mathbf{E}, \mathbf{D}\}$ , we define the macroscopic variables in terms of some suitable surface integrals over the boundary of the  $\mathcal{RVE}$  with volume  $V$ . It should be remarked, that a definition of macroscopic quantities in terms of surface integrals is necessary in general. Respective definitions of macroscopic values by means of simple volume averages could lead to physically unreasonable results and would not allow for reliable interpretations of simple experiments, see e.g. [12]. The

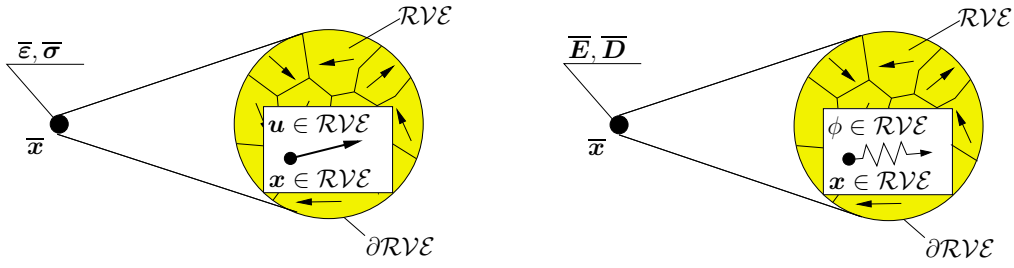


Figure 2: Attached  $\mathcal{RVE}$  at  $\bar{\mathbf{x}}$  associated to the macroscopic mechanical and electrical quantities.

macroscopic strains and stresses are given by

$$\bar{\boldsymbol{\varepsilon}} := \frac{1}{V} \int_{\partial\mathcal{RVE}} \text{sym}[\mathbf{u} \otimes \mathbf{n}] da \quad \text{and} \quad \bar{\boldsymbol{\sigma}} := \frac{1}{V} \int_{\partial\mathcal{RVE}} \text{sym}[\mathbf{t} \otimes \mathbf{x}] da, \quad (3)$$

where  $\mathbf{u}$  and  $\mathbf{t}$  are the displacement and traction vectors on the boundary of the  $\mathcal{RVE}$ , respectively. Furthermore, the macroscopic electric field and electric displacements are defined by the surface integrals

$$\bar{\mathbf{E}} := \frac{1}{V} \int_{\partial\mathcal{RVE}} -\phi \mathbf{n} da \quad \text{and} \quad \bar{\mathbf{D}} := \frac{1}{V} \int_{\partial\mathcal{RVE}} -Q \mathbf{x} da, \quad (4)$$

with the electric potential  $\phi$  and the electric charge density  $Q$  on  $\partial\mathcal{RVE}$ .

## 2.2 Mesoscopic Electro-Mechanically Coupled Boundary Value Problem

On the mesoscopic scale we consider a BVP defined on  $\mathcal{RVE} \subset \mathbb{R}^3$ , which is parameterized in the mesoscopic cartesian coordinates  $\mathbf{x}$ . The governing balance equations are the balance of linear momentum neglecting body forces and Gauß's law neglecting the density of free charge carriers, i.e.

$$\text{div}[\boldsymbol{\sigma}] = \mathbf{0} \quad \text{and} \quad \text{div}[\mathbf{D}] = 0 \quad \forall \mathbf{x} \in \mathcal{RVE}. \quad (5)$$

The mesoscopic strains and electric field vector are given by

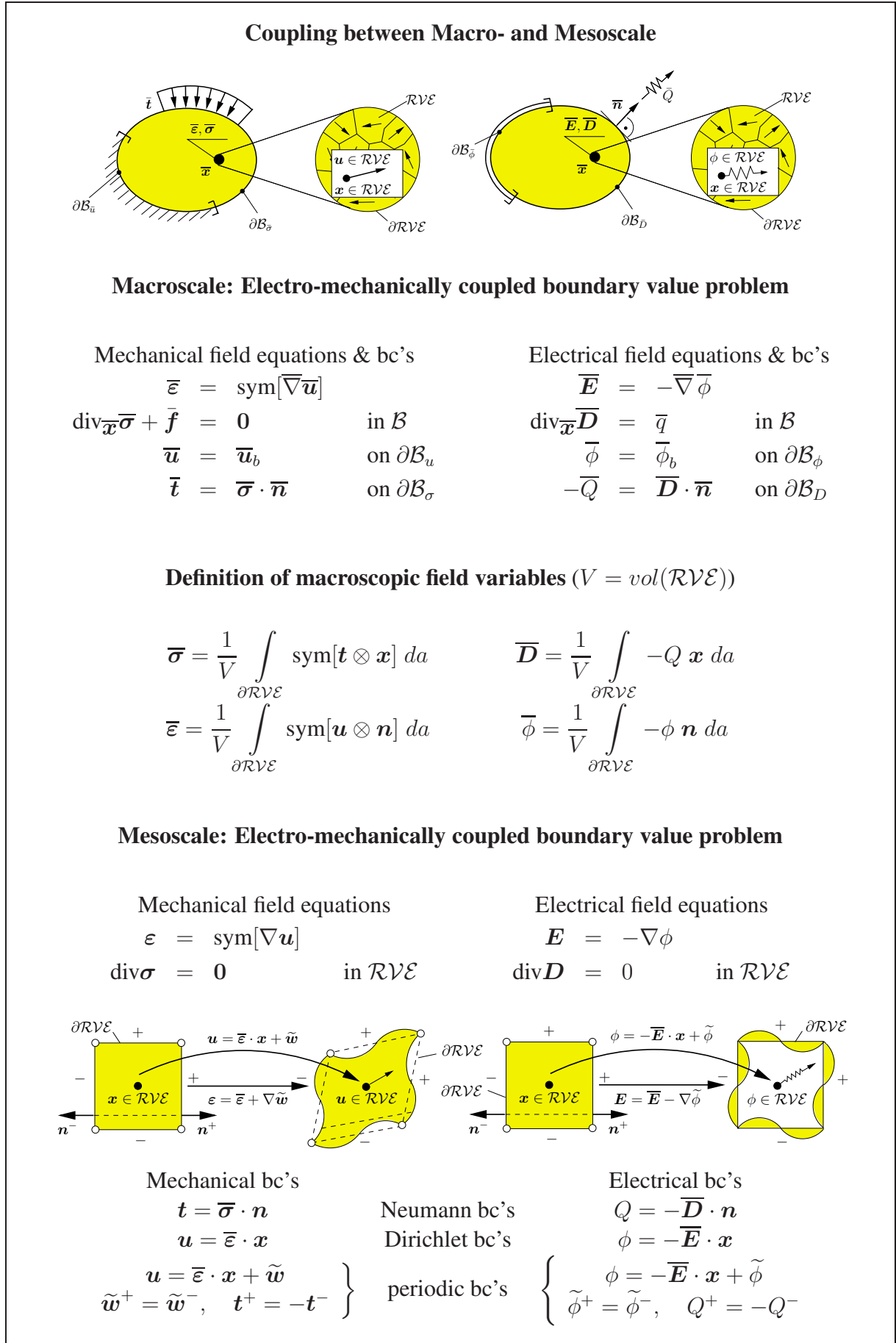
$$\boldsymbol{\varepsilon} := \text{sym}[\nabla \mathbf{u}(\mathbf{x})] \quad \text{and} \quad \mathbf{E} := -\nabla \phi(\mathbf{x}), \quad (6)$$

where  $\nabla$  denotes the gradient operator and  $\text{div}$  the divergence operator with respect to  $\mathbf{x}$ . In order to complete the description of the mesoscopic BVP we have to define some appropriate boundary conditions on  $\partial\mathcal{RVE}$  or some constraint conditions in the whole  $\mathcal{RVE}$ . In order to do so, we apply a generalized macro-homogeneity condition

$$\bar{\boldsymbol{\sigma}} : \dot{\bar{\boldsymbol{\varepsilon}}} + \bar{\mathbf{D}} \cdot \dot{\bar{\mathbf{E}}} = \frac{1}{V} \int_{\mathcal{RVE}} \boldsymbol{\sigma} : \dot{\boldsymbol{\varepsilon}} dv + \frac{1}{V} \int_{\mathcal{RVE}} \mathbf{D} \cdot \dot{\mathbf{E}} dv, \quad (7)$$

which can be utilized to derive suitable boundary conditions on  $\partial\mathcal{RVE}$ , in this context see [18]. The resulting boundary conditions can be prescribed in terms of the Neumann boundary conditions  $\mathbf{t} = \bar{\boldsymbol{\sigma}} \cdot \mathbf{n}$  and  $Q = -\bar{\mathbf{D}} \cdot \mathbf{n}$ , the Dirichlet boundary conditions  $\mathbf{u} = \bar{\boldsymbol{\varepsilon}} \cdot \mathbf{x}$  and  $\phi = -\bar{\mathbf{E}} \cdot \mathbf{x}$ , or in terms of the periodic boundary conditions  $\mathbf{u} = \bar{\boldsymbol{\varepsilon}} \cdot \mathbf{x} + \tilde{\mathbf{w}}$  and  $\phi = -\bar{\mathbf{E}} \cdot \mathbf{x} + \tilde{\phi}$ , with  $\tilde{\mathbf{w}}^+(\mathbf{x}^+) = \tilde{\mathbf{w}}^-(\mathbf{x}^-)$ ,  $\mathbf{t}^+(\mathbf{x}^+) = -\mathbf{t}^-(\mathbf{x}^-)$  and  $\tilde{\phi}^+(\mathbf{x}^+) = \tilde{\phi}^-(\mathbf{x}^-)$ ,  $Q^+(\mathbf{x}^+) = -Q^-(\mathbf{x}^-)$ , respectively. The expressions labelled with a tilde denote the microscopic fluctuation fields and  $\mathbf{x}^\pm$  denote the associated points on the corresponding periodic boundaries (+, -). For convenience, the set of equations of the two-scale homogenization procedure including possible boundary conditions on  $\partial\mathcal{RVE}$  is listed in Table 1.

Table 1: Basic equations of the two-scale homogenization procedure.



### 3. Effective Properties of Piezoelectric Materials

In order to achieve quadratic convergence of the Newton-Raphson iteration scheme of the discretized boundary value problem on the macroscale, we have to perform a consistent linearization of the macroscopic stresses and electric displacements w.r.t. the macroscopic strains and electric field. That means, that we need the macroscopic (overall) mechanical moduli  $\bar{\mathbb{C}}$ , piezoelectric moduli  $\bar{\mathbf{e}}$ , and dielectric moduli  $\bar{\boldsymbol{\epsilon}}$ , which enter the incremental constitutive relations

$$\begin{aligned}\Delta\bar{\boldsymbol{\sigma}} &= \bar{\mathbb{C}} : \Delta\bar{\boldsymbol{\varepsilon}} - \bar{\mathbf{e}}^T \Delta\bar{\mathbf{E}}, \\ -\Delta\bar{\mathbf{D}} &= -\bar{\mathbf{e}} : \Delta\bar{\boldsymbol{\varepsilon}} - \bar{\boldsymbol{\epsilon}} \Delta\bar{\mathbf{E}}.\end{aligned}\quad (8)$$

Formally, we obtain the overall moduli by partial differentiation of the volume averages of the mesoscopic stresses and electric displacements w.r.t. the macroscopic strains and electric field

$$\begin{bmatrix} \Delta\bar{\boldsymbol{\sigma}} \\ -\Delta\bar{\mathbf{D}} \end{bmatrix} = \frac{1}{V} \begin{bmatrix} \partial_{\bar{\boldsymbol{\varepsilon}}} \left\{ \int_{\mathcal{R}\mathcal{V}\mathcal{E}} \boldsymbol{\sigma} \, dv \right\} & \partial_{\bar{\mathbf{E}}} \left\{ \int_{\mathcal{R}\mathcal{V}\mathcal{E}} \boldsymbol{\sigma} \, dv \right\} \\ -\partial_{\bar{\boldsymbol{\varepsilon}}} \left\{ \int_{\mathcal{R}\mathcal{V}\mathcal{E}} \mathbf{D} \, dv \right\} & -\partial_{\bar{\mathbf{E}}} \left\{ \int_{\mathcal{R}\mathcal{V}\mathcal{E}} \mathbf{D} \, dv \right\} \end{bmatrix} \begin{bmatrix} \Delta\bar{\boldsymbol{\varepsilon}} \\ \Delta\bar{\mathbf{E}} \end{bmatrix}. \quad (9)$$

For the analysis of the mesoscopic BVP we conduct an additive decomposition of the mesoscopic strains and electric field into a constant part and a fluctuating part, i.e.  $\boldsymbol{\varepsilon} = \text{sym}[\nabla\mathbf{u}(\mathbf{x})] = \bar{\boldsymbol{\varepsilon}} + \tilde{\boldsymbol{\varepsilon}}$  and  $\mathbf{E} = -\nabla\phi = \bar{\mathbf{E}} + \tilde{\mathbf{E}}$ . Exploiting these relations in (9) leads after application of the chain rule to

$$\begin{bmatrix} \Delta\bar{\boldsymbol{\sigma}} \\ -\Delta\bar{\mathbf{D}} \end{bmatrix} = \frac{1}{V} \left( \int_{\mathcal{R}\mathcal{V}\mathcal{E}} \begin{bmatrix} \mathbb{C} & -\mathbf{e}^T \\ -\mathbf{e} & -\boldsymbol{\epsilon} \end{bmatrix} dv + \int_{\mathcal{R}\mathcal{V}\mathcal{E}} \begin{bmatrix} \mathbb{C} : \partial_{\tilde{\boldsymbol{\varepsilon}}} \tilde{\boldsymbol{\varepsilon}} & -\mathbf{e}^T \cdot \partial_{\tilde{\mathbf{E}}} \tilde{\mathbf{E}} \\ -\mathbf{e} : \partial_{\tilde{\boldsymbol{\varepsilon}}} \tilde{\boldsymbol{\varepsilon}} & -\boldsymbol{\epsilon} \cdot \partial_{\tilde{\mathbf{E}}} \tilde{\mathbf{E}} \end{bmatrix} dv \right) \begin{bmatrix} \Delta\bar{\boldsymbol{\varepsilon}} \\ \Delta\bar{\mathbf{E}} \end{bmatrix}.$$

After some manipulations this leads to the algorithmic expression for the macroscopic, overall electro-mechanical tangent moduli

$$\begin{aligned}\begin{bmatrix} \bar{\mathbb{C}} & -\bar{\mathbf{e}}^T \\ -\bar{\mathbf{e}} & -\bar{\boldsymbol{\epsilon}} \end{bmatrix} &= \frac{1}{V} \int_{\mathcal{R}\mathcal{V}\mathcal{E}} \begin{bmatrix} \mathbb{C} & -\mathbf{e}^T \\ -\mathbf{e} & -\boldsymbol{\epsilon} \end{bmatrix} dv \\ &- \frac{1}{V} \begin{bmatrix} \mathbf{L}_{uu}^T & \mathbf{L}_{\phi u}^T \\ \mathbf{L}_{u\phi}^T & \mathbf{L}_{\phi\phi}^T \end{bmatrix} \begin{bmatrix} \mathbf{K}_{uu} & \mathbf{K}_{u\phi} \\ \mathbf{K}_{\phi u} & \mathbf{K}_{\phi\phi} \end{bmatrix}^{-1} \begin{bmatrix} \mathbf{L}_{uu} & \mathbf{L}_{u\phi} \\ \mathbf{L}_{\phi u} & \mathbf{L}_{\phi\phi} \end{bmatrix}.\end{aligned}\quad (10)$$

with the global, assembled finite element stiffness and L-matrices

$$\begin{aligned}K_{uu} &= \mathbf{A} \mathbf{k}_{uu}^e, & K_{u\phi} &= \mathbf{A} \mathbf{k}_{u\phi}^e, & K_{\phi u} &= \mathbf{A} \mathbf{k}_{\phi u}^e, & K_{\phi\phi} &= \mathbf{A} \mathbf{k}_{\phi\phi}^e, \\ L_{uu} &= \mathbf{A} \mathbf{l}_{uu}^e, & L_{u\phi} &= \mathbf{A} \mathbf{l}_{u\phi}^e, & L_{\phi u} &= \mathbf{A} \mathbf{l}_{\phi u}^e, & L_{\phi\phi} &= \mathbf{A} \mathbf{l}_{\phi\phi}^e,\end{aligned}\quad (11)$$

which result from the matrices of the individual finite elements

$$\begin{aligned}
\mathbf{l}_{uu}^e &= \int_{\mathcal{B}^e} \mathbf{B}_u^{eT} \mathbb{C} \, dv, & \mathbf{k}_{uu}^e &= \int_{\mathcal{B}^e} \mathbf{B}_u^{eT} \mathbb{C} \mathbf{B}^e \, dv, & \mathbf{l}_{u\phi}^e &= - \int_{\mathcal{B}^e} \mathbf{B}_u^{eT} \mathbf{e}^T \, dv, \\
\mathbf{k}_{u\phi}^e &= \int_{\mathcal{B}^e} \mathbf{B}_u^{eT} \mathbf{e}^T \mathbf{B}_\phi^e \, dv, & \mathbf{l}_{\phi u}^e &= \int_{\mathcal{B}^e} \mathbf{B}_\phi^{eT} \cdot \mathbf{e} \, dv, & \mathbf{k}_{\phi u}^e &= \int_{\mathcal{B}^e} \mathbf{B}_\phi^{eT} \mathbf{e} \mathbf{B}_u^e \, dv, \\
\mathbf{l}_{\phi\phi}^e &= \int_{\mathcal{B}^e} \mathbf{B}_\phi^{eT} \boldsymbol{\epsilon} \, dv, & \mathbf{k}_{\phi\phi}^e &= - \int_{\mathcal{B}^e} \mathbf{B}_\phi^{eT} \boldsymbol{\epsilon} \mathbf{B}^e \, dv.
\end{aligned} \tag{12}$$

Here,  $\mathbf{B}_{\phi,u}$  denote the B-matrices comprising the derivatives of the element shape functions,  $\mathbb{C}$  denotes the fourth-order elasticity tensor,  $\mathbf{e}$  is the third-order tensor of piezoelectric moduli and  $\boldsymbol{\epsilon}$  is the second-order tensor of dielectric moduli. For a more detailed derivation of the expressions for the overall moduli the reader is referred to [23] and [24].

#### 4. Transversely Isotropic Mesoscopic Material Model

The utilized material model is given in terms of a coordinate-invariant representation of the quadratic electric enthalpy function as presented in [20]. In this connection we focus on transversely isotropic solids, where  $\mathbf{a}$  with  $\|\mathbf{a}\| = 1$  is the preferred direction of the transversely isotropic material. In the present case of linear piezoelectric material behavior we obtain the general expressions of the stresses and electric displacements as

$$\left. \begin{aligned} \boldsymbol{\sigma} &= \mathbb{C} : \boldsymbol{\epsilon} - \mathbf{e}^T \cdot \mathbf{E} \\ \mathbf{D} &= \mathbf{e} : \boldsymbol{\epsilon} + \boldsymbol{\epsilon} \cdot \mathbf{E} \end{aligned} \right\} \text{ and } \left\{ \begin{aligned} \sigma_{ij} &= \mathbb{C}_{ijkl} \epsilon_{kl} - e_{kij} E_k \\ D_i &= e_{ikl} \epsilon_{kl} + \epsilon_{ik} E_k \end{aligned} \right. \tag{13}$$

in direct and tensorial notation, respectively. The coordinate invariant representation of the mechanical moduli appears as

$$\mathbb{C} = \lambda \mathbf{1} \otimes \mathbf{1} + 2\mu \mathbb{I} + \alpha_3 [\mathbf{1} \otimes \mathbf{m} + \mathbf{m} \otimes \mathbf{1}] + 2\alpha_2 \mathbf{m} \otimes \mathbf{m} + \alpha_1 \boldsymbol{\Xi}, \tag{14}$$

where  $\mathbf{m} = \mathbf{a} \otimes \mathbf{a}$  denotes the second-order structural tensor,  $\mathbf{1}$  the second-order unity tensor,  $\mathbb{I}$  the fourth-order unity tensor and  $\boldsymbol{\Xi}_{ijkl} := [a_i \delta_{jk} a_l + a_k \delta_{il} a_j]$ . The second-order tensor of dielectric moduli is given by

$$\boldsymbol{\epsilon} = -2\gamma_1 \mathbf{1} - 2\gamma_2 \mathbf{m} \tag{15}$$

and the third-order tensor of the piezoelectric moduli appears in the form

$$\mathbf{e} := -\beta_1 \mathbf{a} \otimes \mathbf{1} - \beta_2 \mathbf{a} \otimes \mathbf{m} - \beta_3 \bar{\mathbf{e}} \tag{16}$$

with the abbreviation  $\{\bar{\mathbf{e}}\}_{kij} := \frac{1}{2} [a_i \delta_{kj} + a_j \delta_{ki}]$ . The mesoscopic material parameters are taken from [25] and fitted to the underlying transversely isotropic material model by means of a least-squares approximation. The corresponding mechanical moduli in coordinate-invariant setting appear as

$$\lambda = 108, \quad \mu = 57, \quad \alpha_1 = -53, \quad \alpha_2 = 14.5, \quad \alpha_3 = 3, \tag{17}$$

in units  $GPa$ , the components of the dielectric tensor  $\boldsymbol{\epsilon}$  are

$$\gamma_1 = -9.74, \quad \gamma_2 = 9.49,$$

in units  $10^{-9} C/Vm$ , and the piezoelectric components in units  $C/m^2$  are

$$\beta_1 = 0.7, \quad \beta_2 = 61, \quad \beta_3 = -68.4.$$

## 5. Computation of Effective Electro-Mechanical Moduli of 2-Dimensional Mesostructure

In the following a convergence study of the effective electro-mechanical moduli of a heterogeneous mesostructure is conducted. In detail, we analyze an academic two-dimensional mesoscopic structure, which is composed of a piezoelectric matrix with a piezoelectric inclusion. The matrix is poled in positive  $x_2$ -direction, while the inclusion is polarized in positive  $x_1$ -direction. The mesoscopic BVP is discretized with four separate and increasing mesh densities consisting of 500, 1552, 6876, and 12450 linear triangular finite elements, from which the first three discretizations are depicted in Fig. 3.

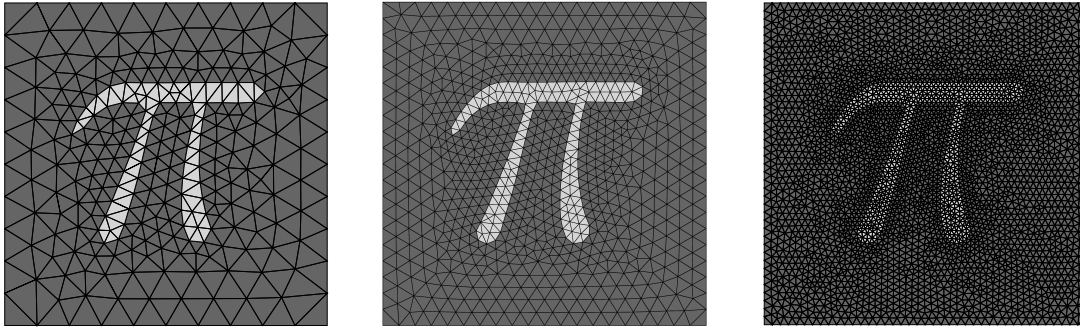


Figure 3: Discretizations of the mesostructure with 500, 1552, and 6876 linear triangles.

The results of the convergence study with periodic boundary conditions are depicted in Fig. 4. As can be seen, the effective macroscopic moduli converge with increasing number of elements on the mesolevel. It should be noted that the presented method is also applicable for the computation of effective parameters of three-dimensional mesostructures, see e.g. [24] and [26].

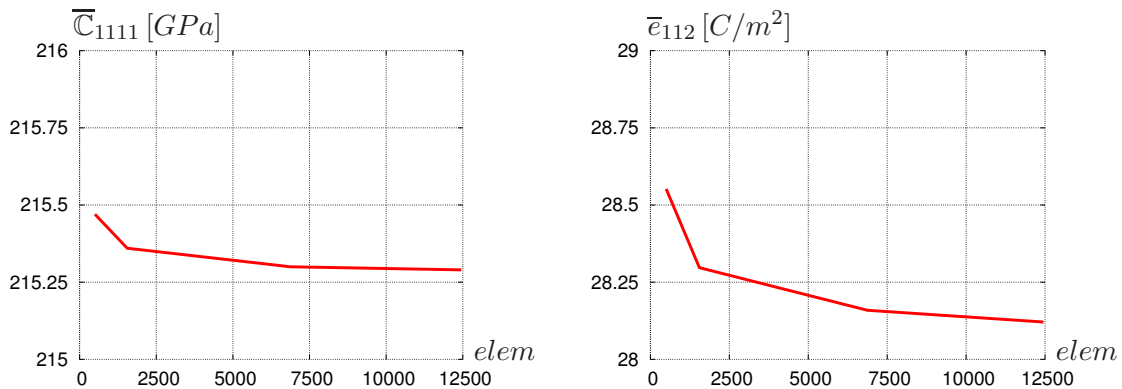


Figure 4: Overall mechanical modul  $\bar{C}_{1111}$  and piezoelectric modul  $\bar{e}_{112}$  vs. number of elements.

## 6. Conclusion

A two-scale homogenization approach for the analysis of electro-mechanically coupled boundary value problems was presented. In this context, a meso-macro transition procedure for electro-mechanically coupled materials in two and three dimensions was derived and implemented into an FE<sup>2</sup>-homogenization environment. The strategy allows for the computation of macroscopic boundary value problems under consideration of attached mesoscopic representative volume elements and can moreover be utilized for the efficient and accurate determination of effective electro-mechanical parameters.

## References

- [1] Z. Hashin and S. Shtrikman. On some variational principles in anisotropic and nonhomogeneous elasticity. *Journal of the Mechanics and Physics of Solids*, 10:335–342, 1962.
- [2] L. J. Walpole. On bounds for the overall elastic moduli of inhomogeneous system. *Journal of the Mechanics and Physics of Solids*, 14:151–162, 1966.
- [3] E. Kröner. Bounds for effective elastic moduli of disordered materials. *Journal of the Mechanics and Physics of Solids*, 25:137–155, 1977.
- [4] J.R. Willis. Bounds and self-consistent estimates for the overall properties of anisotropic composites. *Journal of the Mechanics and Physics of Solids*, 25:185–202, 1966.
- [5] G. A. Francfort and F. Murat. Homogenization and optimal bounds in linear elasticity. *Archive for Rational Mechanics and Analysis*, 94:307–334, 1986.
- [6] T. Chen. Micromechanical estimates of the overall thermoelectroelastic moduli of multiphase fibrous composites. *International Journal of Solids and Structures*, 31(22):3099–3111, 1994.
- [7] Z. Li, C. Wang, and C. Chen. Effective electromechanical properties of transversely isotropic piezoelectric ceramics with microvoids. *Computational Materials Science*, 27(3):381–392, 2003.
- [8] T.I. Zohdi. On the computation of the coupled thermo-electromagnetic response of continua with particulate microstructure. *International Journal for Numerical Methods in Engineering*, 76(8):1250–1279, 2008.
- [9] R.J.M. Smit, W.A.M. Brekelmans, and H.E.H. Meijer. Prediction of the mechanical behavior of nonlinear heterogeneous systems by multi-level finite element modeling. *Computer Methods in Applied Mechanics and Engineering*, 155:181–192, 1998.
- [10] C. Miehe, J. Schröder, and J. Schotte. Computational homogenization analysis in finite plasticity simulation of texture development in polycrystalline materials. *Computer Methods in Applied Mechanics and Engineering*, 171(3-4):387–418, 1999.
- [11] C. Miehe, J. Schotte, and J. Schröder. Computational micro-macro transitions and overall moduli in the analysis of polycrystals at large strains. *Computational Materials Science*, 16(1-4):372–382, 1999. ISSN 0927-0256.
- [12] J. Schröder. *Homogenisierungsmethoden der nichtlinearen Kontinuumsmechanik unter Beachtung von Instabilitäten*. Bericht aus der Forschungsreihe des Instituts für Mechanik (Bauwesen), Lehrstuhl I, Universität Stuttgart, 2000.
- [13] K. Terada and N. Kikuchi. A class of general algorithms for multi-scale analyses of heterogeneous media. *Computer Methods in Applied Mechanics and Engineering*, 190(40-41):5427–5464, 2001. ISSN 0045-7825.
- [14] C. Miehe and A. Koch. Computational micro-to-macro transitions of discretized microstructures undergoing small strains. *Archive of Applied Mechanics*, 72(4):300–317, 2002.
- [15] Z. Xia, Y. Zhang, and F. Ellyin. A unified periodical boundary conditions for representative volume elements of composites and applications. *International Journal of Solids and Structures*, 40:1907–1921, 2003.

- [16] T.I. Zohdi and P. Wriggers. Introduction to computational micromechanics. In F. Pfeiffer and P. Wriggers, editors, *Lecture Notes in Applied and Computational Mechanics*, volume 20. Springer, 2005. ISBN 3540228209.
- [17] D. Markovic, R. Niekamp, A. Ibrahimbegovic, H.G. Matthies, and R.L. Taylor. Multi-scale modeling of heterogeneous structures with inelastic constitutive behavior. *International Journal for Computer-Aided Engineering and Software*, 22(5/6):664–683, 2005.
- [18] J. Schröder. Derivation of the localization and homogenization conditions for electro-mechanically coupled problems. *Computational Materials Science*, 46(3):595–599, 2009. ISSN 0927-0256.
- [19] D.C. Lupascu, J. Schröder, C.S. Lynch, W. Kreher, and I. Westram. *Handbook of Multifunctional Polycrystalline Ferroelectric Materials*, chapter Mechanical Properties of Ferro-Piezoceramics. Springer, Heidelberg, in print.
- [20] J. Schröder and D. Gross. Invariant formulation of the electromechanical enthalpy function of transversely isotropic piezoelectric materials. *Archive of Applied Mechanics*, 73(8): 533–552, 2004.
- [21] H. Romanowski and J. Schröder. Coordinate invariant modelling of the ferroelectric hysteresis within a thermodynamically consistent framework. A mesoscopic approach. In Y. Wang and K. Hutter, editors, *Trends in Applications of Mathematics and Mechanics*, pages 419–428. Shaker Verlag, Aachen, 2005.
- [22] H. Romanowski. *Kontinuumsmechanische Modellierung ferroelektrischer Materialien im Rahmen der Invariantentheorie*. PhD thesis, Institut für Mechanik, Fakultät Ingenieurwissenschaften, Abteilung Bauwissenschaften, Universität Duisburg-Essen, 2006.
- [23] J. Schröder and M.-A. Keip. Computation of the overall properties of microheterogeneous piezoelectric materials. in preparation.
- [24] J. Schröder and M.-A. Keip. *Computer Methods in Mechanics*, volume 1, chapter A Framework for the Two-Scale Homogenization of Electro-Mechanically Coupled Boundary Value Problems, pages 311–329. Springer, 2010.
- [25] M. Zgonik, P. Bernasconi, M. Duelli, R. Schlessler, P. Günter, M. H. Garrett, D. Rytz, Y. Zhu, and X. Wu. Dielectric, elastic, piezoelectric, electro-optic, and elasto-optic tensors of BaTiO<sub>3</sub> crystals. *Physical Review B*, 50(9):5941–5949, 1994.
- [26] J. Schröder and M.-A. Keip. Multiscale modeling of electro-mechanically coupled materials: Homogenization procedure and computation of overall moduli. In *IUTAM-Symposium on "Multiscale Modelling of Fatigue, Damage and Fracture in Smart Materials Systems"*. Kluwer, to appear.

# Using Density Functional Theory to Design New Materials. From Nanoelectronics to the Origin of the Universe

**Nicola A. Spaldin**

Materials Department, University of California, Santa Barbara, CA 93106-5050, USA  
[nicola@mrl.ucsb.edu](mailto:nicola@mrl.ucsb.edu)

Modern computational methods are proving to be invaluable in the first-principles design of new materials with specific targeted functionalities. After discussing the capabilities and limitations of current computational tools, I will illustrate their utility with two examples from the field of multiferroics: First, the design of new materials for electric-field control of magnetism, and second, an experiment to test extensions to the Standard Model by measuring the dipole moment of the electron.

Towards *ab initio* Device Design  
Mark van Schilfgaarde, Arizona State University

A new type of self-consistent scheme within the  $GW$  approximation is presented, which we call the quasiparticle self-consistent  $GW$  (QSGW) approximation. It is based on a kind of self-consistent perturbation theory, where the self-consistency is constructed to minimize the perturbation. QSGW describes optical properties in a wide range of materials rather well, including cases where the local-density and LDA-based  $GW$  approximations fail qualitatively. Self-consistency dramatically improves agreement with experiment, and is sometimes essential. QSGW avoids some formal and practical problems encountered in conventional self-consistent  $GW$ , which will be discussed. QSGW is a true *ab initio* method, which handles both itinerant and correlated electrons on an equal footing, without any ambiguity about how a localized state is defined, or how double-counting terms should be subtracted. Weakly correlated materials such as Na and  $sp$  semiconductors are described with uniformly high accuracy. Discrepancies with experiment are small and systematic, and can be explained in terms of the approximations made.

Its consistently high accuracy make QSGW a versatile method that can reliably predict critical energy band properties of GaAs, CuInSe<sub>2</sub>, TiO<sub>2</sub> and NiO in a unified framework. Also optical response can be calculated, as can scattering matrix elements such as the Auger recombination process. Thus it can serve as an engine for true *ab initio* device design.

The challenge is to map rigorous QSGW results into high-quality reduced hamiltonians that can be applied at the many-atom scale. Some examples will be given: (1) QSGW results are fed into a Monte Carlo Boltzmann Transport Equation solver to simulate a realistic GaAs MESFET without any empirical parameters. (2) A reduced hamiltonian is generated from QSGW to calculate the Rashba spin splitting in GaAs/AlAs. (3) A magnetic hamiltonian is derived from QSGW calculations in Mn:GaAs and used to predict magnetic properties of DMS alloys.

# Micromechanical modeling of ferroelectric thin films within a multiscale simulation chain

Olena Vedmedenko<sup>1</sup>, Th. Steinkopff<sup>1</sup> and B. Kaltenbacher<sup>2</sup>

<sup>1</sup>Siemens AG, Corporate Technology, Global Technology Field Ceramics,  
Otto-Hahn-Ring 6, 81739 Munich, Germany

<sup>2</sup>Karl-Franzens-Universität Graz, Institut für Mathematik und Wissenschaftliches  
Rechnen, Heinrichstraße 36, 8010 Graz, Austria  
[thorsten.steinkopff@siemens.com](mailto:thorsten.steinkopff@siemens.com)

The aim of the multiscale simulation project COMFEM is the predictive description of electromechanical properties of ferroelectric ceramic materials, such as lead zirconate titanate (PZT), lead titanate (PTO) or barium titanate (BTO). Recently, several modeling results on the piezo- and dielectric coefficients of ceramic thin films have been published. These approaches use experimental single crystal data as the input parameters and yield effective material coefficients depending on the saturation angle of polarization. However, for lack of detailed knowledge of the saturation angle and the polarization state at the remanence point the direct comparison of the theoretical and the experimental data is questionable. Moreover, experimental single crystal data for PZT are not available.

To shed light on the described problem we calculated the evolution of polarization configurations and dielectric and piezoelectric properties during the poling process on the basis of the micromechanical Huber-Fleck model. Single crystal data obtained by ab-initio and phase field simulations have been used as input parameters for calculations on PZT and PTO thin films. Furthermore, experimental single crystal data have been applied to simulations of PTO and BTO samples. The Huber-Fleck calculations have been performed for idealistic and realistic 3D grain models, which have been produced by means of a novel grain and mesh generator. The generator is able to render a given grain size distribution and to create periodic extendable grain structures with a spare number of finite elements.

The calculated effective dielectric and piezoelectric constants  $d_{33}^*$  and  $\epsilon_{33}^*$  as well as the remnant polarizations for the BTO, PTO and PZT samples lie in the range of the corresponding experimental values. Thus, the proposed method gives a fair estimation of the required quantities and can be used for prediction of material properties.

Acknowledgement: This work was funded by the German Federal Ministry of Education and Research (BMBF Framework Programme WING, Project Code 03X0510).

# Phase field modeling for ferroelectric materials in the context of a multiscale simulation chain

**Benjamin Voelker<sup>1</sup>, Magalie Huttin<sup>1</sup> and Marc Kamlah<sup>2</sup>**

<sup>1</sup> IZBS, Karlsruhe Institut of Technology, Kaiserstr. 12, 76131 Karlsruhe, Germany

<sup>2</sup> IMF II, Karlsruhe Institut of Technology, Herrmann-von-Helmholtz-Platz 1, 76344 Eggenstein-Leopoldshafen, Germany

[benjamin.voelker@kit.edu](mailto:benjamin.voelker@kit.edu)

In a multiscale simulation approach for ferroelectric materials, thermodynamically motivated phase field simulations can be used to close the gap between predictive ab-initio methods and micromechanical modeling.

The fundament of the phase field theory is a Helmholtz free energy function that contains all crystallographic and boundary information of the ferroelectric material. Different forms of these energy functions that describe both tetragonal and rhombohedral polarized states were taken from literature and examined. Here, higher-order polarization terms were of special interest because of their profoundly sensitive impact. The influence of all inbound parameters of the free energy was analyzed in a sensitivity study. The common way to adjust the parameters of the Helmholtz free energy function is a phenomenological approach relying on experimental results. For the knowledge-based simulation chain, we developed a new adjustment method, which is solely based on results of predictive first-principle calculations and shell-model simulations. These input parameters are the dielectric, piezoelectric and elastic properties, the spontaneous strain and polarization as well as both the 90° and 180° domain wall energy and thickness. Using these parameters it was possible to adjust Helmholtz free energy functions for both PbTiO<sub>3</sub> and PZT.

To link phase field modeling and micromechanical modeling in the simulation chain, the phase field theory was numerically implemented in the finite-element-platform COMSOL Multiphysics. A 2D-periodically continued model with additional degrees of freedom for both the polarization and mechanical displacement in out-of-plane-direction was used to analyze various PbTiO<sub>3</sub> and PZT bulk domain configurations. By applying small external electrical and mechanical loads, the effect of reversible domain wall motion on the small signal parameters was studied. The results of these domain effective calculations provide a basis for micromechanical modeling.

Acknowledgement: This work was funded by the German Federal Ministry of Education and Research (BMBF Framework Programme WING, Project Code 03X0510).

## Switching mechanisms and scaling potential of bipolar redox-based memristive devices

*R. Waser*

*Juelich-Aachen Research Alliance, Section Fundamentals of Future Information Technology (JARA-FIT)  
FZ Juelich and RWTH Aachen, Germany*

There are two different types of bipolar resistive switching cells which utilize redox processes on the nanoscale. One type is based on electrochemical oxidation, cation transport in an ionic conductor, and reduction of an electrochemically active electrode metal such as Ag or Cu (electrochemical metallization mechanism, ECM). The other type is based on the drift of oxygen ions in transition metal oxides, a concentration polarization, and a corresponding valence of the cations which leads to an increase or decrease of the electronic partial conductivity (valence change mechanism, VCM). From the conceptional point of view, both types show potentially a scalability to below 10 nm. In addition, both types show faster write/erase times and lower write/erase voltages than NAND Flash. They are known to be compatible with transistors as selector devices. Possible alternatives for passive crossbar areas will be presented.

The talk will cover our own expertise in comparing different deposition techniques, applying a variety of nano-analytical techniques, and supplementing the experimental studies by simulation. Recent progress in the elucidation of the microscopic switching mechanisms will be discussed. Area-dependent switching vs. filamentary switching will be described and their scaling projections will be presented. The talk will also comprise open questions such as the missing physics based guidelines in the “material’s treasure map”, the design rules for the desired defect structure, the route towards an optimization of the switching speed, the endurance, and the retention, the requirement and conductance of an initial cell formation.